symmetry

MDPI

Article

# Size-Dependent Free Vibration of Non-Rectangular Gradient Elastic Thick Microplates

**Bo Zhang [1], Cheng Li [1,2,3], Limin Zhang [1] and Feng Xie [2,*]**

1 Applied Mechanics and Structure Safety Key Laboratory of Sichuan Province, School of Mechanics and Engineering, Southwest Jiaotong University, Chengdu 611756, China
2 School of Rail Transportation, Soochow University, Suzhou 215131, China
3 School of Automotive Engineering, Changzhou Institute of Technology, Changzhou 213032, China
* Correspondence: fengxie@suda.edu.cn

**Abstract:** The free vibration of isotropic gradient elastic thick non-rectangular microplates is analyzed in this paper. To capture the microstructure-dependent effects of microplates, a negative second-order gradient elastic theory with symmetry is utilized. The related equations of motion and boundary conditions are obtained using the energy variational principle. A closed-form solution is presented for simply supported free-vibrational rectangular microplates with four edges. A $C^1$-type differential quadrature finite element (DQFE) is applied to solve the free vibration of thick microplates. The DQ rule is extended to the straight-sided quadrilateral domain through a coordinate transformation between the natural and Cartesian coordinate systems. The Gauss–Lobato quadrature rule and DQ rule are jointly used to discretize the strain and kinetic energies of a generic straight-sided quadrilateral plate element. Selective numerical examples are validated against those available in the literature. Finally, the impact of various parameters on the free vibration characteristics of annular sectorial and triangular microplates is shown. It indicates that the strain gradient and inertia gradient effects can result in distinct changes in both vibration frequencies and mode shapes.

**Keywords:** free vibration; non-rectangular microplates; gradient elastic theory with symmetry; microstructure-dependent effects; differential quadrature finite element



**Citation:** Zhang, B.; Li, C.; Zhang, L.; Xie, F. Size-Dependent Free Vibration of Non-Rectangular Gradient Elastic Thick Microplates. *Symmetry* **2022**, *14*, 2592. https://doi.org/10.3390/sym14122592

Academic Editor: Raffaele Barretta

Received: 21 October 2022
Accepted: 2 December 2022
Published: 7 December 2022



## 1. Introduction

The free vibration of plates and plate assemblies is a hot topic that has continually inspired researchers for well over two centuries. From an engineering perspective, the importance of this topic cannot be overemphasized, particularly for its applications in the aeronautical industry, where the top and bottom skins of an aircraft wing are generally idealized as plate assemblies during the structural design. In the context of the first- or third-order shear deformation theory (FSDT or TSDT), researchers have conducted many numerical studies on the vibration characteristics of thick plates. For example, Bui et al. [1] presented new numerical results of the high-frequency modes of Mindlin plates using an effective shear-locking-free meshless method. Based on a modified FSDT, Nam et al. [2] developed a four-node plate element with nine degrees of freedom per node for the static bending and vibration of two-layer composite plates. Tran et al. [3] presented new finite element results of the static bending at high temperatures and the thermal buckling of sandwich FG plates using a modified TSDT. Thai et al. [4] applied the finite element method to simulate the mechanical, electric, and polarization behaviors of TSDT-based piezoelectric nanoplates resting on elastic foundations subjected to static loads. Doan et al. [5] used the TSDT and phase-field approach to simulate the free vibration response of cracked nanoplates while taking into account the flexoelectric effect. Duc et al. [6] established a phase-field fracture model in the context of a new TSDT to study the buckling behavior of multi-cracked FG plates.

Increasing progress in ultra-precision machining techniques has spawned various small-sized beam/plate-like structures in the past decades. Owing to their excellent mechanical, electrical, and thermal performance, such structures have widely served as the major load-bearing objects in Micro-Electro-Mechanical Systems (MEMSs) [7]. However, at the micron or even submicron level, the critical dimensions (e.g., diameter and thickness) of structural members are usually of the same order as the characteristic dimensions of constituent materials (e.g., grain size, void radius, and dislocation spacing), which could induce the microstructure-dependent effects validated by experiments and simulations on the bending of microbeams [8–10], the torsion of copper microwires [11,12], and the process of wave propagation in superlattice solids [13,14]. Thus, microstructure-dependent effects should be considered in analyzing static and dynamic problems of small-scale beams and plates for the reliability and design accuracy of MEMS devices. Due to the lack of long-range interactions among adjacent material points, classical continuum mechanics fails to capture size-dependent phenomena.

Classical continuum mechanics needs to be improved by introducing the higher-order spatial derivatives of strain, stress, and inertia terms while preserving its powerful homogenizing characteristic. To realize dimensional homogeneity, one or more material length scale parameters (MLSPs) should be used in non-classical constitutive equations. The original work on gradient-type continuum mechanics can be traced back to Cauchy's exploratory study on modeling discrete lattices in the 1850s. After that, the Cosserat brothers clearly defined microrotations and couple stress in the early 20th century. The first renaissance of higher-order continuum mechanics was promoted by the representative works of Koiter [15], Mindlin [16–18], Toupin [19], and others. Early works focused on the construction of a theoretical framework but lacked experimental validation. Some simplified gradient elasticity theories [8,13,20–23] were proposed and partly validated in the 1980s and 1990s for engineering applications. Among these theories, the single-parameter gradient elasticity theory (SGET) formulated by Aifantis, Ru, and Altan [20,21] and the modified strain gradient elasticity theory (MSGT) established by Lam et al. [8] are the most attractive. Based on the SGET and MSGT, the size-dependent Bernoulli–Euler beam [24,25], Timoshenko beam [26], Reddy–Levinson beam [27], Kirchhoff plate [28,29], Mindlin plate [30,31], Reddy plate [32], and Kirchhoff–Love cylindrical shell [33,34] models have been developed to predict the static bending, free vibration, and buckling behaviors of microscale devices. Roudbari et al. [35] and Kong [36] reviewed the recent advances in non-classical continuum mechanics models and provided research insights for future studies.

In addition to two types of gradient effects, size-dependent phenomena are also caused by other physical factors (e.g., nonlocal stress and surface energy effects). Thus, multifactorial size-dependent constitutive models have been developed to understand mechanical behavior among microscale members. Recently, the nonlocal strain gradient theory (NSGT) proposed by Lim et al. has attracted the most attention [37]. The NSGT can be regarded as a unification of Eringen's nonlocal elasticity theory [38] and Aifantis's strain gradient theory [20]. A nonlocal parameter and a strain gradient parameter are used to weigh the importance of the strain gradient and nonlocal effects. Both the stiffening and softening effects of structural members can be captured by the NSGT. Thus, it has been widely used in modeling small-sized structures with two types of size effects ,. For instance, Lu et al. [39] proposed a unified nonlocal strain gradient beam model for analyzing the size-dependent bending and buckling behaviors of nanobeams with different slenderness ratios. Ma et al. [44] studied wave propagation in thermo-electro-magneto-mechanical-elastic nanoshells using the nonlocal strain gradient thin and shear-deformable cylindrical shell models. Lu et al. [45] developed a consistent surface-stress-enriched nonlocal strain gradient model for a rectangular buckled plate, by which the critical buckling loads of SSSS, CCSS, and CCCC nanoplates are determined. Lu et al. [48] derived a nonlocal strain gradient model including surface stress effects to analyze the free vibration of moderately thick FG cylindrical nanoshells.

Although the size-dependent continuum modeling of microstructural members has been well studied, the derived governing differential equations can be solved analytically for extremely limited types of boundaries, loadings, and geometric conditions. The reason is that the higher-order gradients introduced by the model can lead to a remarkable rise in the order of equations of motion and boundary conditions. For instance, the deflection of gradient elastic Kirchhoff plates [28,29] and Kirchhoff–Love cylindrical shells [33,34] requires $C^2$-continuity. The deflection and rotations of gradient elastic Mindlin plates [31,49] require $C^1$-continuity. Moreover, gradient elastic Reddy plates [32] require both the $C^1$-continuity of rotation and the $C^2$-continuity of deflection. These imply extreme difficulty in solving gradient elastic boundary value problems using both analytical and numerical methods. Although some conventional analytical methods, e.g., the assumed mode method [45,48], Navier method [29,39,40,44,50], extended Kantorovich method [51,52], and $p$-version Ritz method [31], have been proposed to solve special gradient elastic boundary value problems, so far, few studies have focused on gradient elastic plates with non-rectangular shapes and sudden changes in edge supports and thicknesses.

Advanced numerical methods for gradient elastic beams and plates have come forth through the hard work of researchers. For example, Thai et al. [53] analyzed the size-dependent mechanical behavior of FG microplates by combining the use of MSGT and isogeometric analysis (IGA). Nguyen et al. [54] investigated the vibration behavior of FG microplates with cracks, strain gradient effects, and micro-inertia effects by means of an extended IGA. According to the four-unknown refined plate theory, Nguyen et al. [55] used the IGA to predict the geometrically nonlinear bending responses of small-scale FG plates. Moreover, Nguyen et al. [56] constructed a novel NURBS-based IGA model to study the static bending, free vibration, and buckling of couple-stress-enriched FG microplates with higher-order shear and normal deformation effects. Niiranen et al. [57] performed an IGA on the Galerkin discretization scheme with $C^2$-continuity to address the sixth-order boundary value problems of gradient elastic Kirchhoff plates. Balobanov et al. [58] proposed a single-parameter gradient elastic Kirchhoff–Love shell model of arbitrary geometry and the associated $H^3$-conforming isogeometric Galerkin method. Although the IGA approach can yield arbitrary-order continuous basis functions, there are still inadequacies in the integration of the weak form and the imposition of essential boundary conditions in such a method. In addition, the basis functions of an IGA model often have a larger support domain than those of the related finite element model, implying less sparse system matrices and higher computational expense. According to SGET-based Kirchhoff plates, Babu and Patel [59] established nonconforming $C^2$-continuous rectangular plate finite elements for studying the free vibration and linear buckling of single-walled graphene sheets. However, since the standard FEM is subjected to higher-order continuity conditions, researchers have committed to seeking other alternative methods. Wang [60] developed a weak-form quadrature element method (QEM) to study the free vibration of nonlocal strain gradient Euler–Bernoulli beams. Ishaquddin and Gopalakrishnan [61] presented a weak-form QEM for SGET-based Euler–Bernoulli beams and Kirchhoff plates. To enhance the adaptability of the DQM, combining the advantages of the DQM and FEM may be a good choice. Zhang et al. [62] utilized the advantages of the DQM and FEM for the first time to construct weak-form DQFEs related to isotropic MSGT-based Euler–Bernoulli and Timoshenko beam models, respectively. Soon afterward, they proposed a series of weak-form DQFEs for size-dependent Reddy beams [63,64], Mindlin plates [65,66], and Kirchhoff plates [67–69] and showed the efficacy of their developed DQFEM in comparison with the standard FEM.

The aim of this article is to study the free vibration of non-rectangular gradient elastic thick microplates with two types of gradient effects. The remainder of the paper is organized as follows. Section 2 applies the energy variational principle to derive the corresponding equations of motion and boundary conditions. Section 3 develops a quadrilateral differential quadrature finite element to solve the resulting higher-order boundary value problems. In Section 4, we highlight the effectiveness of our theoretical model and solution method by comparing it with other available methods and use it to predict the vibrational behavior of annular sectorial and triangular microplates. Finally, we draw conclusions from our research work in Section 5.

## 2. Governing Equations of Gradient Elastic Thick Microplates

An originally flat isotropic microplate with moderate thickness $h$ is illustrated in Figure 1, where the plate midplane $A$ coincides with the $OXY$ coordinate plane, and the bold symbols $\boldsymbol{n}$ and $\boldsymbol{s}$ are the unit normal and tangent vectors at a point on the boundary curve $\partial A$, respectively. The material parameters are as follows: Young's modulus $E$, shear modulus $G$, Poisson's ratio $\nu$, and mass density $\rho$. When the plate receives a transversely distributed load $Q$ on the upper flat surface, there will be a deflection $W$ and two transverse normal rotations $\Phi_X$ and $\Phi_Y$ about the $Y$- and $X$-axes, respectively.

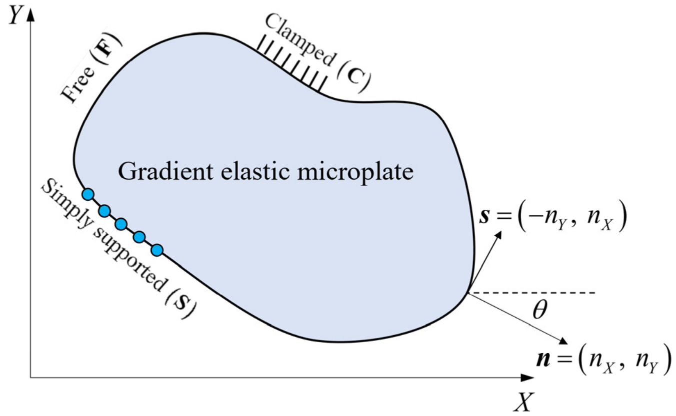


**Figure 1.** Schematic of an isotropic thick gradient elastic microplate.

For a moderately thick microplate, the displacement field is assumed as

$$U_X = Z\Phi_X(X, Y, t), \; U_Y = Z\Phi_Y(X, Y, t), \; U_Z = W(X, Y, t), \tag{1}$$

where $U_X$, $U_Y$, and $U_Z$ are the displacement components along the $X$-, $Y$-, and $Z$-directions, respectively.

The nonzero components of the Cauchy strain tensor are

$$\varepsilon_{XX} = Z\frac{\partial \Phi_X}{\partial X}, \varepsilon_{YY} = Z\frac{\partial \Phi_Y}{\partial Y}, \varepsilon_{XY} = \varepsilon_{YZ} = \frac{Z}{2}\left(\frac{\partial \Phi_X}{\partial Y} + \frac{\partial \Phi_Y}{\partial X}\right), \varepsilon_{ZX} = \varepsilon_{XZ} = \frac{1}{2}\left(\Phi_X + \frac{\partial W}{\partial X}\right), \tag{2}$$

$$\varepsilon_{YZ} = \varepsilon_{ZY} = \frac{1}{2}\left(\Phi_Y + \frac{\partial W}{\partial Y}\right)$$

Second-order gradient elastic theory [20,21] is initiated from the homogenization of lattice structures by applying the Taylor series to approximate the displacement field of a discrete model. For the negative form, the related constitutive relation is expressed in the following symmetrical form:

$$\sigma_{ij} = C_{ijkl}\left(\varepsilon_{kl} - l_s^2 \nabla^2 \varepsilon_{kl}\right) \tag{3}$$

where $C_{ijkl}$ denotes the elastic constitutive tensor with double symmetry, $l_s$ is the static length scale parameter, $\nabla^2$ is the Laplace operator, Latin subscripts run over the symbols $X$, $Y$, and $Z$ unless otherwise indicated, and $\varepsilon_{kl}$ is the Cauchy strain tensor.

The exploration of the plane stress conditions and Equations (2) and (3) yield the stress–strain equations for gradient elastic Mindlin microplates as follows:

$$\begin{array}{l}\sigma_{XX}=\frac{E}{1-\nu^2}\left(1-l_s^2\nabla^2\right)(\varepsilon_{XX}+\nu\varepsilon_{YY})=\left(1-l_s^2\nabla^2\right)\hat{\sigma}_{XX}.\\ \sigma_{XY}=\frac{E}{1+\nu}\left(1-l_s^2\nabla^2\right)\varepsilon_{XY}=\left(1-l_s^2\nabla^2\right)\hat{\sigma}_{XY},\\ \sigma_{YY}=\frac{E}{1-\nu^2}\left(1-l_s^2\nabla^2\right)(\varepsilon_{YY}+\nu\varepsilon_{XX})=\left(1-l_s^2\nabla^2\right)\hat{\sigma}_{YY}.\\ \sigma_{XZ}=\frac{E}{1+\nu}\left(1-l_s^2\nabla^2\right)\varepsilon_{XZ}=\left(1-l_s^2\nabla^2\right)\hat{\sigma}_{XZ},\\ \sigma_{YZ}=\frac{E}{1+\nu}\left(1-l_s^2\nabla^2\right)\varepsilon_{YZ}=\left(1-l_s^2\nabla^2\right)\hat{\sigma}_{YZ}\end{array} \tag{4}$$

where $\hat{\sigma}_{XX}$, $\hat{\sigma}_{XY}$, $\hat{\sigma}_{YY}$, $\hat{\sigma}_{XZ}$, and $\hat{\sigma}_{YZ}$ are classical stresses, and $E$ and $\nu$ are Young's modulus and Poisson's ratio, respectively.

Based on Equations (2)–(4) and [28], the strain energy of the present microplate is expressed as

$$\begin{array}{l}\Pi_s=\frac{1}{2}\int_\Omega(\hat{\sigma}_{XX}\varepsilon_{XX}+\hat{\sigma}_{YY}\varepsilon_{YY}+2\hat{\sigma}_{XY}\varepsilon_{XY}+2K_s\hat{\sigma}_{YZ}\varepsilon_{YZ}+2K_s\hat{\sigma}_{XZ}\varepsilon_{XZ})\mathrm{d}\Omega+\\ \frac{l_s^2}{2}\int_\Omega\left(\begin{array}{l}\frac{\partial\hat{\sigma}_{XX}}{\partial X}\frac{\partial\varepsilon_{XX}}{\partial X}+\frac{\partial\hat{\sigma}_{XX}}{\partial Y}\frac{\partial\varepsilon_{XX}}{\partial Y}+\frac{\partial\hat{\sigma}_{YY}}{\partial X}\frac{\partial\varepsilon_{YY}}{\partial X}+\frac{\partial\hat{\sigma}_{YY}}{\partial Y}\frac{\partial\varepsilon_{YY}}{\partial Y}+2\frac{\partial\hat{\sigma}_{XY}}{\partial X}\frac{\partial\varepsilon_{XY}}{\partial X}\\ +2\frac{\partial\hat{\sigma}_{XY}}{\partial Y}\frac{\partial\varepsilon_{XY}}{\partial Y}+2K_s\frac{\partial\hat{\sigma}_{YZ}}{\partial X}\frac{\partial\varepsilon_{YZ}}{\partial X}+2K_s\frac{\partial\hat{\sigma}_{YZ}}{\partial Y}\frac{\partial\varepsilon_{YZ}}{\partial Y}+2K_s\frac{\partial\hat{\sigma}_{XZ}}{\partial X}\frac{\partial\varepsilon_{XZ}}{\partial X}\\ +2K_s\frac{\partial\hat{\sigma}_{XZ}}{\partial Y}\frac{\partial\varepsilon_{XZ}}{\partial Y}\end{array}\right)\mathrm{d}\Omega\\ =\frac{1}{2}\int_A\left\{\Gamma_1\left[\left(\Phi_X+\frac{\partial W}{\partial X}\right)^2+\left(\Phi_Y+\frac{\partial W}{\partial Y}\right)^2\right]+\Gamma_2\left(\frac{\partial\Phi_X}{\partial Y}+\frac{\partial\Phi_Y}{\partial X}\right)^2+\Gamma_3\frac{\partial\Phi_X}{\partial X}\frac{\partial\Phi_Y}{\partial Y}\right.\\ +\Gamma_4\left[\left(\frac{\partial\Phi_X}{\partial X}\right)^2+\left(\frac{\partial\Phi_Y}{\partial Y}\right)^2\right]+\Gamma_5\left(\frac{\partial\Phi_X}{\partial X}+\frac{\partial^2W}{\partial X^2}\right)^2+\Gamma_5\left(\frac{\partial\Phi_Y}{\partial X}+\frac{\partial^2W}{\partial X\partial Y}\right)^2\\ +\Gamma_5\left(\frac{\partial\Phi_X}{\partial Y}+\frac{\partial^2W}{\partial X\partial Y}\right)^2+\Gamma_5\left(\frac{\partial^2W}{\partial Y^2}+\frac{\partial\Phi_Y}{\partial Y}\right)^2+\Gamma_6\left(\frac{\partial^2\Phi_X}{\partial X\partial Y}+\frac{\partial^2\Phi_Y}{\partial X^2}\right)^2+\\ +\Gamma_6\left(\frac{\partial^2\Phi_X}{\partial Y^2}+\frac{\partial^2\Phi_Y}{\partial X\partial Y}\right)^2+\Gamma_8\left(\frac{\partial^2\Phi_X}{\partial X\partial Y}\frac{\partial^2\Phi_Y}{\partial Y^2}+\frac{\partial^2\Phi_Y}{\partial X\partial Y}\frac{\partial^2\Phi_X}{\partial X^2}\right)+\\ \left.\Gamma_7\left[\left(\frac{\partial^2\Phi_X}{\partial X\partial Y}\right)^2+\left(\frac{\partial^2\Phi_Y}{\partial X\partial Y}\right)^2+\left(\frac{\partial^2\Phi_Y}{\partial Y^2}\right)^2+\left(\frac{\partial^2\Phi_X}{\partial X^2}\right)^2\right]\right\}\mathrm{d}A\end{array} \tag{5}$$

where

$$\begin{array}{l}\Gamma_1=\frac{K_sEh}{4(1+\nu)},\ \Gamma_2=\frac{Eh^3}{48(1+\nu)},\ \Gamma_3=\frac{E\nu\,h^3}{12(1-\nu^2)},\ \Gamma_4=\frac{Eh^3}{24(1-\nu^2)},\ \Gamma_5=\frac{K_sEhl_s^2}{4(1+\nu)},\\ \Gamma_6=\frac{Eh^3l_s^2}{48(1+\nu)},\ \Gamma_7=\frac{Eh^3l_s^2}{24(1-\nu^2)},\ \Gamma_8=\frac{Eh^3\nu\,l_s^2}{12(1-\nu^2)},\end{array} \tag{6}$$

where $K_s$ is the shear correction factor. Equation (5) can reduce to its counterpart (see Equation (10) in [66]) when $\Sigma_1=\Gamma_5$, $\Sigma_{15}=\Sigma_5=\Sigma_2=0$, $\Sigma_3+\Sigma_{17}=\Gamma_3$, $\Sigma_4+\Sigma_{16}=\Gamma_4+\Gamma_5$, $\Sigma_{18}=\Gamma_2-\Gamma_5$, $\Sigma_{12}=2\,\Gamma_6$, $\Sigma_8=\Sigma_7=\Sigma_6=2\,\Gamma_5$, $\Sigma_9=\Gamma_1$, $\Sigma_{10}=\Gamma_6+\Gamma_7$, $\Sigma_{11}=\Gamma_8$, $\Sigma_{13}=\Gamma_7$, and $\Sigma_{14}=\Gamma_6$.

To capture the inertia gradient effect, the contribution of the velocity gradient should be considered. On the basis of [13,57], the kinetic energy of the present microplate is as follows:

$$\begin{array}{l}\Pi_d=\int_\Omega\frac{\rho}{2}\left(\frac{\partial U_X}{\partial t}\frac{\partial U_X}{\partial t}+l_d^2\frac{\partial^2U_X}{\partial X\partial t}\frac{\partial^2U_X}{\partial X\partial t}+l_d^2\frac{\partial^2U_Y}{\partial Y\partial t}\frac{\partial^2U_Y}{\partial Y\partial t}+l_d^2\frac{\partial^2U_Z}{\partial Z\partial t}\frac{\partial^2U_Z}{\partial Z\partial t}\right)\mathrm{d}\Omega\\ =\frac{1}{2}\int_A\left\{\begin{array}{l}\rho\,h\left(\frac{\partial W}{\partial t}\right)^2+\frac{\rho\,h^3}{12}\left(\frac{\partial\Phi_X}{\partial t}\right)^2+\frac{\rho\,h^3}{12}\left(\frac{\partial\Phi_Y}{\partial t}\right)^2+\\ \rho hl_d^2\left[\left(\frac{\partial\Phi_X}{\partial t}\right)^2+\left(\frac{\partial\Phi_Y}{\partial t}\right)^2+\left(\frac{\partial^2W}{\partial X\partial t}\right)^2+\left(\frac{\partial^2W}{\partial Y\partial t}\right)^2\right]+\\ \frac{\rho l_d^2h^3}{12}\left[\left(\frac{\partial^2\Phi_X}{\partial t\partial X}\right)^2+\left(\frac{\partial^2\Phi_X}{\partial t\partial Y}\right)^2+\left(\frac{\partial^2\Phi_Y}{\partial t\partial X}\right)^2+\left(\frac{\partial^2\Phi_Y}{\partial t\partial Y}\right)^2\right]\end{array}\right\}\mathrm{d}A\end{array} \tag{7}$$

where $l_d$ is the dynamic length scale parameter.

Similar to the derivation process in [28,30], the virtual work done by external forces is written as the following equation:

$$\begin{aligned}\delta\Pi_e = &\int_A Q\delta W \mathrm{d}X\mathrm{d}Y + \int_{\partial A} \overline{V}_{(W)}\delta W \mathrm{d}s + \int_{\partial A} \overline{M}_{(W)}\frac{\partial \delta W}{\partial n}\mathrm{d}s + \int_{\partial A} \overline{V}_{(\Phi_s)}\delta\Phi_s \mathrm{d}s \\ &+ \int_{\partial A} \overline{M}_{(\Phi_s)}\frac{\partial \delta\Phi_s}{\partial n}\mathrm{d}s + \int_{\partial A} \overline{V}_{(\Phi_n)}\delta\Phi_n \mathrm{d}s + \int_{\partial A} \overline{M}_{(\Phi_n)}\frac{\partial \delta\Phi_n}{\partial n}\mathrm{d}s\end{aligned} \tag{8}$$

where $Q$ is the distributed transverse load, $\overline{V}_{(W)}$, $\overline{V}_{(\Phi_s)}$, and $\overline{V}_{(\Phi_n)}$ are generalized shear forces, and $\overline{M}_{(W)}$, $\overline{M}_{(\Phi_s)}$, and $\overline{M}_{(\Phi_n)}$ are generalized bending moments.

The displacement-based equations of motion and boundary conditions of gradient elastic thick microplates can be obtained using the variational formulations provided in [69].

For any $(X,\ Y) \in A$ and $t \in (t_1,\ t_2)$:

$$\begin{aligned}&Q + 2\Gamma_1\left(\frac{\partial\Phi_X}{\partial X} + \frac{\partial\Phi_Y}{\partial Y}\right) - 2\Gamma_5\left(\frac{\partial^4 W}{\partial X^4} + 2\frac{\partial^4 W}{\partial Y^2\partial X^2} + \frac{\partial^4 W}{\partial Y^4}\right) + 2\Gamma_1\left(\frac{\partial^2 W}{\partial X^2} + \frac{\partial^2 W}{\partial Y^2}\right) \\ &-2\Gamma_5\left(\frac{\partial^3\Phi_X}{\partial X^3} + \frac{\partial^3\Phi_Y}{\partial X^2\partial Y} + \frac{\partial^3\Phi_X}{\partial X\partial Y^2} + \frac{\partial^3\Phi_Y}{\partial Y^3}\right) - \rho h\frac{\partial^2 W}{\partial t^2} + \rho h l_d^2\left(\frac{\partial^4 W}{\partial X^2\partial t^2} + \frac{\partial^4 W}{\partial Y^2\partial t^2}\right) = 0,\end{aligned} \tag{9}$$

$$\begin{aligned}&\Gamma_3\frac{\partial^2\Phi_Y}{\partial X\partial Y} + 2\Gamma_4\frac{\partial^2\Phi_X}{\partial X^2} - 2\Gamma_1\left(\Phi_X + \frac{\partial W}{\partial X}\right) + 2\Gamma_2\left(\frac{\partial^2\Phi_X}{\partial Y^2} + \frac{\partial^2\Phi_Y}{\partial X\partial Y}\right) - \Gamma_8\left(\frac{\partial^4\Phi_Y}{\partial X^3\partial Y} + \frac{\partial^4\Phi_Y}{\partial X\partial Y^3}\right) \\ &+2\Gamma_5\left(\frac{\partial^3 W}{\partial X^3} + \frac{\partial^3 W}{\partial X\partial Y^2} + \frac{\partial^2\Phi_X}{\partial X^2} + \frac{\partial^2\Phi_X}{\partial Y^2}\right) - 2\Gamma_6\left(\frac{\partial^4\Phi_X}{\partial X^2\partial Y^2} + \frac{\partial^4\Phi_Y}{\partial X^3\partial Y} + \frac{\partial^4\Phi_X}{\partial Y^4} + \frac{\partial^4\Phi_Y}{\partial X\partial Y^3}\right) \\ &-\rho h\left(\frac{h^2}{12} + l_d^2\right)\frac{\partial^2\Phi_X}{\partial t^2} - 2\Gamma_7\left(\frac{\partial^4\Phi_X}{\partial X^4} + \frac{\partial^4\Phi_X}{\partial X^2\partial Y^2}\right) + \frac{\rho h^3 l_d^2}{12}\left(\frac{\partial^4\Phi_X}{\partial X^2\partial t^2} + \frac{\partial^4\Phi_X}{\partial Y^2\partial t^2}\right) = 0,\end{aligned} \tag{10}$$

$$\begin{aligned}&\Gamma_3\frac{\partial^2\Phi_X}{\partial X\partial Y} + 2\Gamma_4\frac{\partial^2\Phi_Y}{\partial Y^2} - 2\Gamma_1\left(\Phi_Y + \frac{\partial W}{\partial Y}\right) + 2\Gamma_2\left(\frac{\partial^2\Phi_Y}{\partial X^2} + \frac{\partial^2\Phi_X}{\partial X\partial Y}\right) - \Gamma_8\left(\frac{\partial^4\Phi_X}{\partial X\partial Y^3} + \frac{\partial^4\Phi_X}{\partial X^3\partial Y}\right) \\ &+2\Gamma_5\left(\frac{\partial^3 W}{\partial Y^3} + \frac{\partial^3 W}{\partial X^2\partial Y} + \frac{\partial^2\Phi_Y}{\partial Y^2} + \frac{\partial^2\Phi_Y}{\partial X^2}\right) - 2\Gamma_6\left(\frac{\partial^4\Phi_Y}{\partial X^2\partial Y^2} + \frac{\partial^4\Phi_X}{\partial X^3\partial Y} + \frac{\partial^4\Phi_Y}{\partial X^4} + \frac{\partial^4\Phi_X}{\partial X\partial Y^3}\right) \\ &-\rho h\left(\frac{h^2}{12} + l_d^2\right)\frac{\partial^2\Phi_Y}{\partial t^2} - 2\Gamma_7\left(\frac{\partial^4\Phi_Y}{\partial X^2\partial Y^2} + \frac{\partial^4\Phi_Y}{\partial Y^4}\right) + \frac{\rho h^3 l_d^2}{12}\left(\frac{\partial^4\Phi_Y}{\partial X^2\partial t^2} + \frac{\partial^4\Phi_Y}{\partial Y^2\partial t^2}\right) = 0.\end{aligned} \tag{11}$$

Because of the introduction of higher-order partial derivatives and boundary conditions, the present model is difficult to solve using an analytical or semi-analytical method. The available works focus on seeking analytical/numerical solutions for gradient elastic beams and plates with simple loading and boundary conditions.

## 3. Solution Procedure

### *3.1. Navier Method*

For a simply supported gradient elastic rectangular microplate, the Navier method can be used to derive the analytical free vibration solution. In this case, $W$, $\Phi_X$, and $\Phi_Y$ can be written as

$$\begin{aligned}W &= \sum_{m=1}^{\infty}\sum_{n=1}^{\infty} A_{mn}e^{j\omega t}\sin(\alpha_m X)\sin(\beta_n Y), \\ \Phi_X &= \sum_{m=1}^{\infty}\sum_{n=1}^{\infty} B_{mn}e^{j\omega t}\cos(\alpha_m X)\sin(\beta_n Y), \\ \Phi_Y &= \sum_{m=1}^{\infty}\sum_{n=1}^{\infty} C_{mn}e^{j\omega t}\sin(\alpha_m X)\cos(\beta_n Y),\end{aligned} \tag{12}$$

where $A_{mn}$, $B_{mn}$, and $C_{mn}$ are Fourier coefficients, $\omega$ is the vibration frequency, $j$ is the imaginary unit, $L_X$ and $L_Y$ are the length and width of a rectangular microplate, respectively, and $\alpha_m = m\pi/L_X\beta_n = n\pi/L_Y$. The following expression is obtained by substituting Equation (12) into Equations (9)–(11).

$$\left\{\begin{bmatrix} K_{11}^{(mn)} & K_{12}^{(mn)} & K_{13}^{(mn)} \\ K_{21}^{(mn)} & K_{22}^{(mn)} & K_{23}^{(mn)} \\ K_{31}^{(mn)} & K_{32}^{(mn)} & K_{33}^{(mn)} \end{bmatrix} - \omega^2 \begin{bmatrix} M_{11}^{(mn)} & M_{12}^{(mn)} & M_{13}^{(mn)} \\ M_{21}^{(mn)} & M_{22}^{(mn)} & M_{23}^{(mn)} \\ M_{31}^{(mn)} & M_{32}^{(mn)} & M_{33}^{(mn)} \end{bmatrix}\right\}\begin{bmatrix} A_{mn} \\ B_{mn} \\ C_{mn} \end{bmatrix} = \begin{bmatrix} 0 \\ 0 \\ 0 \end{bmatrix}, \tag{13}$$

where

$$\begin{aligned}
K_{21}^{(mn)} &= K_{12}^{(mn)} = 2\,\Gamma_1\alpha_m + 2\,\Gamma_5\alpha_m\left(\alpha_m^2+\beta_n^2\right),\\
K_{31}^{(mn)} &= K_{13}^{(mn)} = 2\Gamma_1\beta_n + 2\Gamma_5\,\beta_n\left(\alpha_m^2+\beta_n^2\right),\\
K_{22}^{(mn)} &= 2\,\Gamma_1 + 2(\Gamma_4\,+\Gamma_5\,)\alpha_m^2 + 2\,(\Gamma_2+\Gamma_5)\beta_n^2 + 2\,\left(\alpha_m^2+\beta_n^2\right)\left(\beta_n^2\Gamma_6+\alpha_m^2\Gamma_7\right),\\
K_{23}^{(mn)} &= (\Gamma_3+2\,\Gamma_2)\alpha_m\beta_n + (\Gamma_8+2\Gamma_6)\alpha_m^3\beta_n + (\Gamma_8+2\Gamma_6)\alpha_m\beta_n^3,
\end{aligned} \tag{14}$$

$$M_{11}^{(mn)} = \rho h + \rho h l_d^2\left(\alpha_m^2+\beta_n^2\right),\ M_{33}^{(mn)} = M_{22}^{(mn)} = \frac{\rho h^3}{12} + \rho h l_d^2 + \frac{\rho l_d^2 h^3}{12}\left(\alpha_m^2+\beta_n^2\right). \tag{15}$$

For a non-trivial solution of $A_{mn}$, $B_{mn}$, and $C_{mn}$, it is required that the determinant of the coefficient matrix of Equation (13) vanish. The determinant of the coefficient matrix in Equation (13) is a cubic equation in $\omega^2$, the smallest (positive) root of which gives the $mn$th natural frequency, $\omega_{mn}$, for the free vibration of the plate.

*3.2. Differential Quadrature Finite Element Method (DQFEM)*

A quadrilateral DQFE is derived to address the general free vibration problem of the present gradient elastic model. Figure 2 illustrates a 2D DQ-based geometric mapping scheme to satisfy the $C^1$-continuity conditions of $W$, $\Phi_X$, and $\Phi_Y$ and a natural-to-Cartesian coordinate transformation to make the DQ rule feasible for a straight-sided quadrilateral domain.

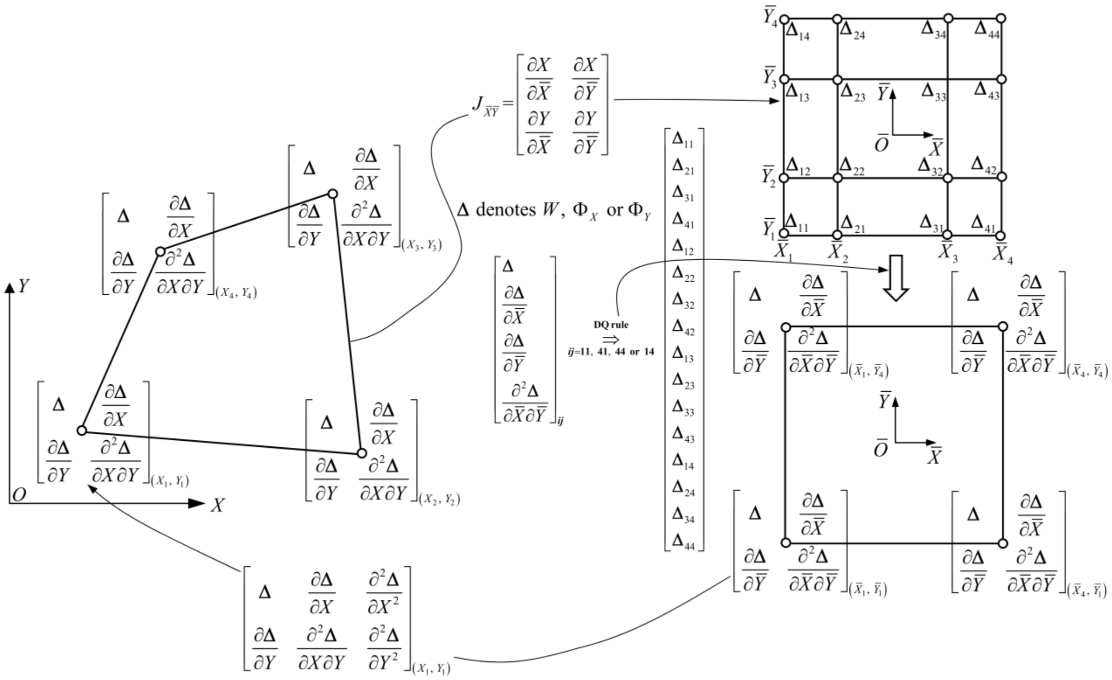


**Figure 2.** Diagram of a 2D DQ-based geometric mapping scheme and a natural-to-Cartesian geometric mapping scheme [67].

From Figure 2, we can derive the partial derivative relationship between the global and local coordinate systems as follows:

$$\begin{bmatrix}\frac{\partial}{\partial \overline{X}}\\ \frac{\partial}{\partial \overline{Y}}\end{bmatrix} = \boldsymbol{J}_{\overline{XY}}^{-1}\begin{bmatrix}\frac{\partial}{\partial X}\\ \frac{\partial}{\partial Y}\end{bmatrix},\ \begin{bmatrix}\frac{\partial^2}{\partial \overline{X}^2}\\ \frac{\partial^2}{\partial \overline{Y}^2}\\ \frac{\partial^2}{\partial \overline{X}\partial \overline{Y}}\end{bmatrix} = \begin{bmatrix}\left(\frac{\partial \overline{X}}{\partial X}\right)^2 & \left(\frac{\partial \overline{Y}}{\partial X}\right)^2 & 2\frac{\partial \overline{X}}{\partial X}\frac{\partial \overline{Y}}{\partial X}\\ \left(\frac{\partial \overline{X}}{\partial Y}\right)^2 & \left(\frac{\partial \overline{Y}}{\partial Y}\right)^2 & 2\frac{\partial \overline{X}}{\partial Y}\frac{\partial \overline{Y}}{\partial Y}\\ \frac{\partial \overline{X}}{\partial X}\frac{\partial \overline{X}}{\partial Y} & \frac{\partial \overline{Y}}{\partial X}\frac{\partial \overline{Y}}{\partial Y} & \frac{\partial \overline{Y}}{\partial X}\frac{\partial \overline{X}}{\partial Y} + \frac{\partial \overline{X}}{\partial X}\frac{\partial \overline{Y}}{\partial Y}\end{bmatrix}\begin{bmatrix}\frac{\partial^2}{\partial \overline{X}^2}\\ \frac{\partial^2}{\partial \overline{Y}^2}\\ \frac{\partial^2}{\partial \overline{X}\partial \overline{Y}}\end{bmatrix}, \tag{16}$$

where

$$\boldsymbol{J}_{\overline{X}\overline{Y}} = \begin{bmatrix} \frac{\partial X}{\partial \overline{X}} & \frac{\partial Y}{\partial \overline{X}} \\ \frac{\partial X}{\partial \overline{Y}} & \frac{\partial Y}{\partial \overline{Y}} \end{bmatrix}, \; \boldsymbol{J}_{\overline{X}\overline{Y}}^{-1} = \begin{bmatrix} \frac{\partial \overline{X}}{\partial X} & \frac{\partial \overline{Y}}{\partial X} \\ \frac{\partial \overline{X}}{\partial Y} & \frac{\partial \overline{Y}}{\partial Y} \end{bmatrix}. \tag{17}$$

Using Equations (16) and (17), Equation (5) can be transformed into a natural coordinate system:

$$\begin{aligned}
\Pi_s = \int_{-1}^{1}\int_{-1}^{1} \Bigg[ & \beta_1 \left(\frac{\partial^2 W}{\partial \overline{X}^2}\right)^2 + \beta_2 \left(\frac{\partial^2 W}{\partial \overline{Y}^2}\right)^2 + \beta_3 \left(\frac{\partial^2 W}{\partial \overline{X}\partial \overline{Y}}\right)^2 + \beta_4 \frac{\partial^2 W}{\partial \overline{X}^2}\frac{\partial^2 W}{\partial \overline{Y}^2} + \beta_5 \frac{\partial^2 W}{\partial \overline{X}^2}\frac{\partial^2 W}{\partial \overline{X}\partial \overline{Y}} + \\
& \beta_6 \frac{\partial^2 W}{\partial \overline{Y}^2}\frac{\partial^2 W}{\partial \overline{X}\partial \overline{Y}} + \beta_7 \left(\frac{\partial^2 \Phi_X}{\partial \overline{X}^2}\right)^2 + \beta_8 \left(\frac{\partial^2 \Phi_X}{\partial \overline{Y}^2}\right)^2 + \beta_9 \left(\frac{\partial^2 \Phi_X}{\partial \overline{X}\partial \overline{Y}}\right)^2 + \beta_{10} \frac{\partial^2 \Phi_X}{\partial \overline{X}^2}\frac{\partial^2 \Phi_X}{\partial \overline{Y}^2} + \\
& \beta_{11} \frac{\partial^2 \Phi_X}{\partial \overline{X}^2}\frac{\partial^2 \Phi_X}{\partial \overline{X}\partial \overline{Y}} + \beta_{12} \frac{\partial^2 \Phi_X}{\partial \overline{Y}^2}\frac{\partial^2 \Phi_X}{\partial \overline{X}\partial \overline{Y}} + \beta_{13} \left(\frac{\partial^2 \Phi_Y}{\partial \overline{X}^2}\right)^2 + \beta_{14} \left(\frac{\partial^2 \Phi_Y}{\partial \overline{Y}^2}\right)^2 + \beta_{15} \left(\frac{\partial^2 \Phi_Y}{\partial \overline{X}\partial \overline{Y}}\right)^2 \\
& + \beta_{16} \frac{\partial^2 \Phi_Y}{\partial \overline{X}^2}\frac{\partial^2 \Phi_Y}{\partial \overline{Y}^2} + \beta_{17} \frac{\partial^2 \Phi_Y}{\partial \overline{X}^2}\frac{\partial^2 \Phi_Y}{\partial \overline{X}\partial \overline{Y}} + \beta_{18} \frac{\partial^2 \Phi_Y}{\partial \overline{Y}^2}\frac{\partial^2 \Phi_Y}{\partial \overline{X}\partial \overline{Y}} + \beta_{19} \frac{\partial^2 \Phi_X}{\partial \overline{X}^2}\frac{\partial^2 \Phi_Y}{\partial \overline{X}^2} + \\
& \beta_{20} \frac{\partial^2 \Phi_X}{\partial \overline{Y}^2}\frac{\partial^2 \Phi_Y}{\partial \overline{Y}^2} + \beta_{21} \frac{\partial^2 \Phi_X}{\partial \overline{X}^2}\frac{\partial^2 \Phi_Y}{\partial \overline{Y}^2} + \beta_{22} \frac{\partial^2 \Phi_Y}{\partial \overline{X}^2}\frac{\partial^2 \Phi_X}{\partial \overline{Y}^2} + \beta_{23} \frac{\partial^2 \Phi_X}{\partial \overline{X}^2}\frac{\partial^2 \Phi_Y}{\partial \overline{X}\partial \overline{Y}} + \\
& \beta_{24} \frac{\partial^2 \Phi_X}{\partial \overline{Y}^2}\frac{\partial^2 \Phi_Y}{\partial \overline{X}\partial \overline{Y}} + \beta_{25} \frac{\partial^2 \Phi_Y}{\partial \overline{Y}^2}\frac{\partial^2 \Phi_X}{\partial \overline{X}\partial \overline{Y}} + \beta_{26} \frac{\partial^2 \Phi_Y}{\partial \overline{X}^2}\frac{\partial^2 \Phi_X}{\partial \overline{X}\partial \overline{Y}} + \beta_{27} \frac{\partial^2 \Phi_X}{\partial \overline{X}\partial \overline{Y}}\frac{\partial^2 \Phi_Y}{\partial \overline{X}\partial \overline{Y}} + \\
& \beta_{28} \frac{\partial^2 W}{\partial \overline{Y}^2}\frac{\partial \Phi_X}{\partial \overline{Y}} + \beta_{29} \frac{\partial^2 W}{\partial \overline{Y}^2}\frac{\partial \Phi_X}{\partial \overline{X}} + \beta_{30} \frac{\partial^2 W}{\partial \overline{Y}^2}\frac{\partial \Phi_Y}{\partial \overline{Y}} + \beta_{31} \frac{\partial^2 W}{\partial \overline{Y}^2}\frac{\partial \Phi_Y}{\partial \overline{X}} + \beta_{32} \frac{\partial^2 W}{\partial \overline{X}^2}\frac{\partial \Phi_X}{\partial \overline{Y}} \\
& + \beta_{33} \frac{\partial^2 W}{\partial \overline{X}^2}\frac{\partial \Phi_X}{\partial \overline{X}} + \beta_{34} \frac{\partial^2 W}{\partial \overline{X}^2}\frac{\partial \Phi_Y}{\partial \overline{Y}} + \beta_{35} \frac{\partial^2 W}{\partial \overline{X}^2}\frac{\partial \Phi_Y}{\partial \overline{X}} + \beta_{36} \frac{\partial^2 W}{\partial \overline{X}\partial \overline{Y}}\frac{\partial \Phi_X}{\partial \overline{Y}} + \beta_{37} \frac{\partial^2 W}{\partial \overline{X}\partial \overline{Y}}\frac{\partial \Phi_X}{\partial \overline{X}} \\
& + \beta_{38} \frac{\partial^2 W}{\partial \overline{X}\partial \overline{Y}}\frac{\partial \Phi_Y}{\partial \overline{Y}} + \beta_{39} \frac{\partial^2 W}{\partial \overline{X}\partial \overline{Y}}\frac{\partial \Phi_Y}{\partial \overline{X}} + \beta_{40} \frac{\partial \Phi_X}{\partial \overline{Y}}\frac{\partial \Phi_Y}{\partial \overline{Y}} + \beta_{41} \frac{\partial \Phi_Y}{\partial \overline{X}}\frac{\partial \Phi_X}{\partial \overline{Y}} + \beta_{42} \frac{\partial \Phi_X}{\partial \overline{X}}\frac{\partial \Phi_X}{\partial \overline{Y}} \\
& + \beta_{43} \frac{\partial \Phi_X}{\partial \overline{X}}\frac{\partial \Phi_Y}{\partial \overline{Y}} + \beta_{44} \frac{\partial \Phi_X}{\partial \overline{X}}\frac{\partial \Phi_Y}{\partial \overline{X}} + \beta_{45} \frac{\partial \Phi_Y}{\partial \overline{X}}\frac{\partial \Phi_Y}{\partial \overline{Y}} + \beta_{46} \left(\frac{\partial W}{\partial \overline{X}}\right)^2 + \beta_{47} \left(\frac{\partial W}{\partial \overline{Y}}\right)^2 + \\
& \beta_{48} \left(\frac{\partial \Phi_X}{\partial \overline{X}}\right)^2 + \beta_{49} \left(\frac{\partial \Phi_X}{\partial \overline{Y}}\right)^2 + \beta_{50} \left(\frac{\partial \Phi_Y}{\partial \overline{X}}\right)^2 + \beta_{51} \left(\frac{\partial \Phi_Y}{\partial \overline{Y}}\right)^2 + \beta_{52} \frac{\partial W}{\partial \overline{X}}\frac{\partial W}{\partial \overline{Y}} + \beta_{53} \Phi_X \frac{\partial W}{\partial \overline{X}} \\
& + \beta_{54} \Phi_X \frac{\partial W}{\partial \overline{Y}} + \beta_{55} \Phi_Y \frac{\partial W}{\partial \overline{X}} + \beta_{56} \Phi_Y \frac{\partial W}{\partial \overline{Y}} + \beta_{57} \left(\Phi_X^2 + \Phi_Y^2\right) \Bigg] \left|\boldsymbol{J}_{\overline{X}\overline{Y}}\right| \mathrm{d}\overline{X}\mathrm{d}\overline{Y},
\end{aligned} \tag{18}$$

where $\beta_{\mathrm{m}}$ is the coordinate transformation coefficient, as shown in Appendix A.

Based on Equations (7), (16) and (17), the kinetic energy for the gradient elastic thick plate element is rewritten as

$$\Pi_d = \int_{-1}^{1}\int_{-1}^{1} \left\{ \begin{array}{l} \alpha_1 \left(\frac{\partial W}{\partial t}\right)^2 + \alpha_2 \left[\left(\frac{\partial \Phi_X}{\partial t}\right)^2 + \left(\frac{\partial \Phi_Y}{\partial t}\right)^2\right] + \alpha_3 \left(\frac{\partial^2 W}{\partial \overline{X}\partial t}\right)^2 + \\ \alpha_4 \left(\frac{\partial^2 W}{\partial \overline{Y}\partial t}\right)^2 + \alpha_5 \frac{\partial^2 W}{\partial \overline{X}\partial t}\frac{\partial^2 W}{\partial \overline{Y}\partial t} + \alpha_6 \frac{\partial^2 \Phi_Y}{\partial \overline{X}\partial t}\frac{\partial^2 \Phi_Y}{\partial \overline{Y}\partial t} + \\ \alpha_6 \frac{\partial^2 \Phi_X}{\partial \overline{X}\partial t}\frac{\partial^2 \Phi_X}{\partial \overline{Y}\partial t} + \alpha_7 \left[\left(\frac{\partial^2 \Phi_X}{\partial \overline{X}\partial t}\right)^2 + \left(\frac{\partial^2 \Phi_Y}{\partial \overline{X}\partial t}\right)^2\right] + \\ \alpha_8 \left[\left(\frac{\partial^2 \Phi_Y}{\partial \overline{Y}\partial t}\right)^2 + \left(\frac{\partial^2 \Phi_X}{\partial \overline{Y}\partial t}\right)^2\right] \end{array} \right\} \left|\boldsymbol{J}_{\overline{X}\overline{Y}}\right| \mathrm{d}\overline{X}\mathrm{d}\overline{Y}, \tag{19}$$

where

$$\begin{aligned}
& \alpha_1 = \frac{\rho\, h}{2},\; \alpha_2 = \frac{\rho h\left(h^2 + 12 l_d^2\right)}{24},\; \alpha_3 = \frac{\rho h l_d^2}{2} \left[\left(\frac{\partial \overline{X}}{\partial X}\right)^2 + \left(\frac{\partial \overline{X}}{\partial Y}\right)^2\right], \\
& \alpha_4 = \frac{\rho h l_d^2}{2} \left[\left(\frac{\partial \overline{Y}}{\partial X}\right)^2 + \left(\frac{\partial \overline{Y}}{\partial Y}\right)^2\right],\; \alpha_5 = \rho h l_d^2 \left(\frac{\partial \overline{X}}{\partial X}\frac{\partial \overline{Y}}{\partial X} + \frac{\partial \overline{X}}{\partial Y}\frac{\partial \overline{Y}}{\partial Y}\right), \\
& \alpha_6 = \frac{\rho h^3 l_d^2}{12} \left(\frac{\partial \overline{X}}{\partial X}\frac{\partial \overline{Y}}{\partial X} + \frac{\partial \overline{X}}{\partial Y}\frac{\partial \overline{Y}}{\partial Y}\right),\; \alpha_7 = \frac{\rho h^3 l_d^2}{24} \left[\left(\frac{\partial \overline{X}}{\partial X}\right)^2 + \left(\frac{\partial \overline{X}}{\partial Y}\right)^2\right], \\
& \alpha_8 = \frac{\rho h^3 l_d^2}{24} \left[\left(\frac{\partial \overline{Y}}{\partial X}\right)^2 + \left(\frac{\partial \overline{Y}}{\partial Y}\right)^2\right].
\end{aligned} \tag{20}$$

Gauss–Lobatto (GL) quadrature points and weight coefficients in Figure 2 are given by

$$\overline{Y}_1 = \overline{X}_1 = -1,\; \overline{Y}_2 = \overline{X}_2 = -1/\sqrt{5},\; \overline{X}_3 = \overline{Y}_3 = 1/\sqrt{5},\; \overline{X}_4 = \overline{Y}_4 = 1, \tag{21}$$

$$C_1^{(\overline{X})} = C_1^{(\overline{Y})} = C_4^{(\overline{X})} = C_4^{(\overline{Y})} = 1/6,\; C_2^{(\overline{X})} = C_2^{(\overline{Y})} = C_3^{(\overline{X})} = C_3^{(\overline{Y})} = 5/6. \tag{22}$$

Next, the Lagrange interpolation technique is used to obtain the trial functions of $W$,$\Phi_X$, and $\Phi_Y$:

$$\Delta = \sum_{i=1}^{4}\sum_{j=1}^{4} l_{\overline{X}(i)}\left(\overline{X}\right) l_{\overline{Y}(j)}\left(\overline{Y}\right)\Delta_{ij}, \tag{23}$$

where $\Delta_{ij}$ represents the function value of $W$, $\Phi_X$, or $\Phi_Y$ at the $ij$th GL quadrature point; $l_{\overline{X}(i)}\left(\overline{X}\right)$ and $l_{\overline{Y}(j)}\left(\overline{Y}\right)$ are the Lagrange interpolation polynomials along the $\overline{X}$- and $\overline{Y}$-directions, respectively.

For a standard parent domain $[-1,\ 1] \times [-1,\ 1]$, the 1st and 2nd partial derivatives of $W$, $\Phi_X$, and $\Phi_Y$ at all GL quadrature points are expressed as follows:

$$\begin{gathered}
\begin{bmatrix} \boldsymbol{D}_{\overline{X}}^{(1)}\boldsymbol{W}_{(\mathrm{GL})} \\ \boldsymbol{D}_{\overline{X}}^{(1)}\boldsymbol{\Phi}_{X(\mathrm{GL})} \\ \boldsymbol{D}_{\overline{X}}^{(1)}\boldsymbol{\Phi}_{Y(\mathrm{GL})} \end{bmatrix} = \boldsymbol{A}_{\overline{X}}^{(1)} \begin{bmatrix} \boldsymbol{W}_{(\mathrm{GL})} \\ \boldsymbol{\Phi}_{X(\mathrm{GL})} \\ \boldsymbol{\Phi}_{Y(\mathrm{GL})} \end{bmatrix},\ 
\begin{bmatrix} \boldsymbol{D}_{\overline{Y}}^{(1)}\boldsymbol{W}_{(\mathrm{GL})} \\ \boldsymbol{D}_{\overline{Y}}^{(1)}\boldsymbol{\Phi}_{X(\mathrm{GL})} \\ \boldsymbol{D}_{\overline{Y}}^{(1)}\boldsymbol{\Phi}_{Y(\mathrm{GL})} \end{bmatrix} = \boldsymbol{A}_{\overline{Y}}^{(1)} \begin{bmatrix} \boldsymbol{W}_{(\mathrm{GL})} \\ \boldsymbol{\Phi}_{X(\mathrm{GL})} \\ \boldsymbol{\Phi}_{Y(\mathrm{GL})} \end{bmatrix},\ 
\begin{bmatrix} \boldsymbol{D}_{\overline{X}}^{(2)}\boldsymbol{W}_{(\mathrm{GL})} \\ \boldsymbol{D}_{\overline{X}}^{(2)}\boldsymbol{\Phi}_{X(\mathrm{GL})} \\ \boldsymbol{D}_{\overline{X}}^{(2)}\boldsymbol{\Phi}_{Y(\mathrm{GL})} \end{bmatrix} = \boldsymbol{A}_{\overline{X}}^{(2)} \begin{bmatrix} \boldsymbol{W}_{(\mathrm{GL})} \\ \boldsymbol{\Phi}_{X(\mathrm{GL})} \\ \boldsymbol{\Phi}_{Y(\mathrm{GL})} \end{bmatrix}, \\
\begin{bmatrix} \boldsymbol{D}_{\overline{XY}}^{(1\oplus1)}\boldsymbol{W}_{(\mathrm{GL})} \\ \boldsymbol{D}_{\overline{XY}}^{(1\oplus1)}\boldsymbol{\Phi}_{X(\mathrm{GL})} \\ \boldsymbol{D}_{\overline{XY}}^{(1\oplus1)}\boldsymbol{\Phi}_{Y(\mathrm{GL})} \end{bmatrix} = \boldsymbol{A}_{\overline{XY}}^{(1\oplus1)} \begin{bmatrix} \boldsymbol{W}_{(\mathrm{GL})} \\ \boldsymbol{\Phi}_{X(\mathrm{GL})} \\ \boldsymbol{\Phi}_{Y(\mathrm{GL})} \end{bmatrix},\ 
\begin{bmatrix} \boldsymbol{D}_{\overline{Y}}^{(2)}\boldsymbol{W}_{(\mathrm{GL})} \\ \boldsymbol{D}_{\overline{Y}}^{(2)}\boldsymbol{\Phi}_{X(\mathrm{GL})} \\ \boldsymbol{D}_{\overline{Y}}^{(2)}\boldsymbol{\Phi}_{Y(\mathrm{GL})} \end{bmatrix} = \boldsymbol{A}_{\overline{Y}}^{(2)} \begin{bmatrix} \boldsymbol{W}_{(\mathrm{GL})} \\ \boldsymbol{\Phi}_{X(\mathrm{GL})} \\ \boldsymbol{\Phi}_{Y(\mathrm{GL})} \end{bmatrix},
\end{gathered} \tag{24}$$

where $\boldsymbol{D}_{\overline{XY}}^{(p\oplus q)}\boldsymbol{\Delta}_{(\mathrm{GL})}$ is the following partial derivative matrix:

$$\begin{aligned}
\boldsymbol{D}_{\overline{XY}}^{(p\oplus q)}\boldsymbol{\Delta}_{(\mathrm{GL})} = \Bigg[ & \left(\frac{\partial^{p+q}\Delta}{\partial\overline{X}^p\partial\overline{Y}^q}\right)_{11}, \left(\frac{\partial^{p+q}\Delta}{\partial\overline{X}^p\partial\overline{Y}^q}\right)_{21}, \left(\frac{\partial^{p+q}\Delta}{\partial\overline{X}^p\partial\overline{Y}^q}\right)_{31}, \left(\frac{\partial^{p+q}\Delta}{\partial\overline{X}^p\partial\overline{Y}^q}\right)_{41}, \\
& \left(\frac{\partial^{p+q}\Delta}{\partial\overline{X}^p\partial\overline{Y}^q}\right)_{12}, \left(\frac{\partial^{p+q}\Delta}{\partial\overline{X}^p\partial\overline{Y}^q}\right)_{22}, \left(\frac{\partial^{p+q}\Delta}{\partial\overline{X}^p\partial\overline{Y}^q}\right)_{32}, \left(\frac{\partial^{p+q}\Delta}{\partial\overline{X}^p\partial\overline{Y}^q}\right)_{42}, \\
& \left(\frac{\partial^{p+q}\Delta}{\partial\overline{X}^p\partial\overline{Y}^q}\right)_{13}, \left(\frac{\partial^{p+q}\Delta}{\partial\overline{X}^p\partial\overline{Y}^q}\right)_{23}, \left(\frac{\partial^{p+q}\Delta}{\partial\overline{X}^p\partial\overline{Y}^q}\right)_{33}, \left(\frac{\partial^{p+q}\Delta}{\partial\overline{X}^p\partial\overline{Y}^q}\right)_{43}, \\
& \left(\frac{\partial^{p+q}\Delta}{\partial\overline{X}^p\partial\overline{Y}^q}\right)_{14}, \left(\frac{\partial^{p+q}\Delta}{\partial\overline{X}^p\partial\overline{Y}^q}\right)_{24}, \left(\frac{\partial^{p+q}\Delta}{\partial\overline{X}^p\partial\overline{Y}^q}\right)_{34}, \left(\frac{\partial^{p+q}\Delta}{\partial\overline{X}^p\partial\overline{Y}^q}\right)_{44}\Bigg]^{\mathrm{T}}
\end{aligned} \tag{25}$$

with $\left(\frac{\partial^{p+q}\Delta}{\partial\overline{X}^p\partial\overline{Y}^q}\right)_{ij}$ denoting the function value of $\frac{\partial^{p+q}\Delta}{\partial\overline{X}^p\partial\overline{Y}^q}$ at the $ij$th GL quadrature point. $\boldsymbol{W}_{(\mathrm{GL})}$, $\boldsymbol{\Phi}_{X(\mathrm{GL})}$, and $\boldsymbol{\Phi}_{Y(\mathrm{GL})}$ are defined in the following vectors:

$$\Delta_{(\mathrm{GL})} = [\Delta_{11},\ \Delta_{21},\ \Delta_{31},\ \Delta_{41},\ \Delta_{12},\ \Delta_{22},\ \Delta_{32},\ \Delta_{42},\ \Delta_{13},\ \Delta_{23},\ \Delta_{33},\ \Delta_{43},\ \Delta_{14},\ \Delta_{24},\ \Delta_{34},\ \Delta_{44}]^{\mathrm{T}}, \tag{26}$$

and $\boldsymbol{A}_{\overline{X}}^{(1)}$, $\boldsymbol{A}_{\overline{Y}}^{(1)}$, $\boldsymbol{A}_{\overline{X}}^{(2)}$, $\boldsymbol{A}_{\overline{XY}}^{(1\oplus1)}$, and $\boldsymbol{A}_{\overline{Y}}^{(2)}$ are $16 \times 16$ weight coefficient matrices, as detailed in [65].

Based on Equation (22), the following weigh coefficient matrix $\boldsymbol{C}_{(\mathrm{GL})}$ formed at all quadrature points is defined:

$$\boldsymbol{C}_{(\mathrm{GL})} = diag([1,\ 5,\ 5,\ 1,\ 5,\ 25,\ 25,\ 5, 5,\ 25,\ 25,\ 5,\ 1,\ 5,\ 5,\ 1])/36, \tag{27}$$

The element stiffness and mass matrices and load vector are determined using the same discretization procedure as depicted in [66,70]. Based on the previous work in [57], we divide the clamped and simply supported boundaries into two types according to the normal curvature, i.e., single and double attributes.

Simply supported (S):

$$\text{Single attribute}:\ W = \Phi_s = 0 \tag{28}$$

$$\text{Double attribute}: \; W = \Phi_s = \frac{\partial \Phi_n}{\partial n} = 0 \tag{29}$$

Clamped (C):

$$\text{Single attribute}: \; W = \Phi_s = \Phi_n = 0 \tag{30}$$

$$\text{Double attribute}: \; W = \Phi_s = \Phi_n = \frac{\partial \Phi_n}{\partial n} = 0 \tag{31}$$

Free (F): No constraint.

## 4. Numerical Results and Discussion

### *4.1. Model Validation*

The convergence and accuracy of our model are verified by some selective examples. The vibration frequencies predicted by the *pb*-2 Ritz method for thick macroplates and by the Navier method for thick microplates are used as benchmarks.

Figures 3 and 4 illustrate three mesh densities for an annular sectorial plate and an equilateral triangular plate, respectively. For the annular sectorial case, $\overline{\omega}_n = \omega R_{\text{out}}^2 \sqrt{\rho h / D}$, inner radius $R_{\text{in}} = 0.5$, outer radius $R_{\text{out}} = 1.0$, $h = 0.1$, sectorial angle $\alpha = 45^{\circ}$, $\nu = 0.3$, and $K_s = 5/6$; for the equilateral triangular plate, $\overline{\omega}_n = \omega L^2 \sqrt{\rho h / D}$, side length $L = 1.0$, $h = 0.1$, $\nu = 0.3$, and $K_s = \pi^2/12$. Note that $D = Eh^3 / \left[12\left(1-\nu^2\right)\right]$ is the flexural rigidity of the thin plate.

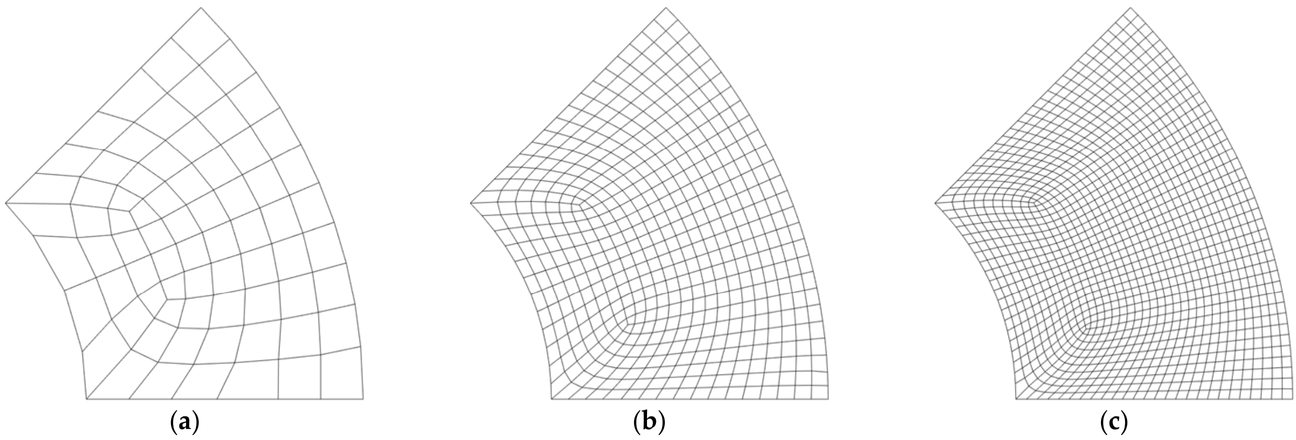


**Figure 3.** Three types of meshing for an annular sectorial plate [67]: (**a**) I: 86 nodes and 72 elements; (**b**) II: 536 nodes and 500 elements; (**c**) III: 1297 nodes and 1240 elements.

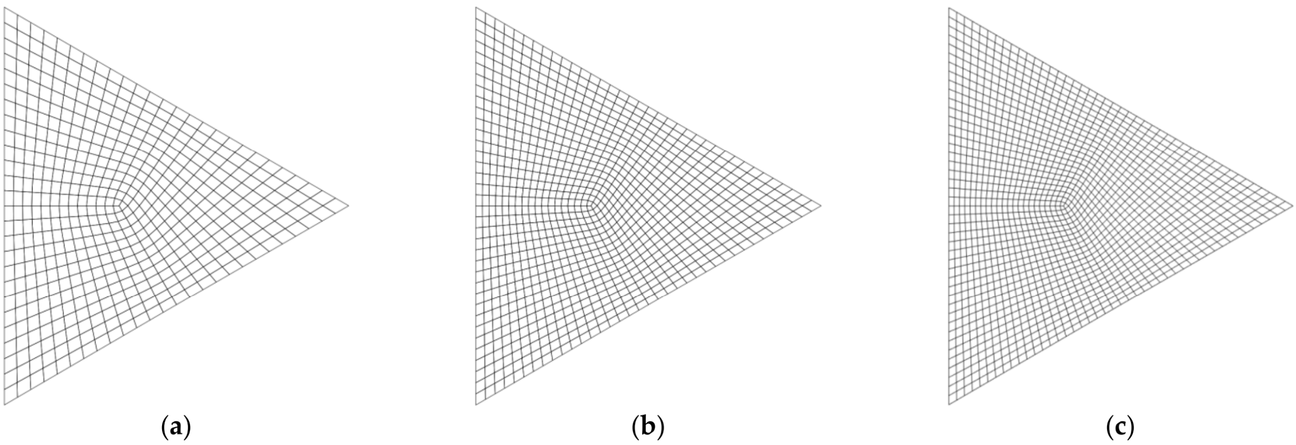


**Figure 4.** Three types of meshing for an equilateral triangular plate: (**a**) I: 547 nodes and 507 elements; (**b**) II: 1027 nodes and 972 elements; (**c**) III: 1519 nodes and 1452 elements.

The six lowest dimensionless frequencies for two macroplates under three types of meshing are shown in Tables 1 and 2. It is expected that the predicted frequency parameters converge to their counterparts using the *pb*-2 Ritz method [71] and ABAQUS (8-node curved thick shell element) as mesh density increases. The use of Mesh III can produce good accuracy since the maximum relative error between the proposed method and the reported results in [71] is less than 1‰. However, it can be observed that the change in the boundary conditions affects the convergence error. To further validate the effectiveness of our method, we provide the six lowest vibration mode shapes in the form of deflection contour plots for two macroplates (Figures 5 and 6). As expected, the present contour plots are in agreement with those obtained by ABAQUS.

**Table 1.** The six lowest dimensionless frequencies for an annular sectorial macroplate with three types of meshing (single attribute).

| Plate Type | Source | Dimensionless Frequency | | | | | |
|---|---|---|---|---|---|---|---|
| | | $\bar{\omega}_1$ | $\bar{\omega}_2$ | $\bar{\omega}_3$ | $\bar{\omega}_4$ | $\bar{\omega}_5$ | $\bar{\omega}_6$ |
| 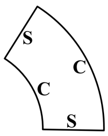 | Mesh I | 81.6282 | 131.5274 | 170.5684 | 204.4813 | 213.2321 | 273.2040 (19.7‰) |
| | Mesh II | 83.3317 | 133.4009 | 173.9067 | 207.6397 | 217.9088 | 278.5504 (0.54‰) |
| | Mesh III | 83.3762 | 133.5073 | 173.9903 | 207.7985 | 218.1862 | 278.6688 (0.11‰) |
| | Ref. [71] | 83.39 | 133.5 | 174.0 | 207.8 | 218.2 | 278.7 (0.00‰) |
| | ABAQUS | 83.4149 | 133.6469 | 174.2138 | 208.1828 | 218.3593 | 278.9532 |
| 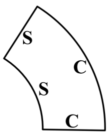 | Mesh I | 79.7667 | 139.6404 | 163.5869 | 212.3000 | 215.0767 | 267.0375 (13.5‰) |
| | Mesh II | 80.7754 | 142.1242 | 165.5137 | 217.2101 | 218.9190 | 270.4049 (1.10‰) |
| | Mesh III | 80.9566 | 142.2275 | 165.6100 | 217.3999 | 219.1845 | 270.5344 (0.61‰) |
| | Ref. [71] | 81.01 | 142.2 | 165.8 | 217.4 | 219.3 | 270.7 (0.00‰) |
| | ABAQUS | 81.1477 | 142.8058 | 166.1301 | 217.8956 | 220.0316 | 270.9513 |

**Table 2.** The six lowest dimensionless frequencies for an equilateral triangular macroplate with three types of meshing (single attribute).

| Plate Type | Source | Dimensionless Frequency | | | | | |
|---|---|---|---|---|---|---|---|
| | | $\bar{\omega}_1$ | $\bar{\omega}_2$ | $\bar{\omega}_3$ | $\bar{\omega}_4$ | $\bar{\omega}_5$ | $\bar{\omega}_6$ |
| 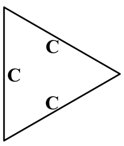 | Mesh I | 77.6961 | 132.1974 | 132.1974 | 188.2262 | 196.6173 | 196.6173 (1.94‰) |
| | Mesh II | 77.7317 | 132.2817 | 132.2817 | 188.3909 | 196.8075 | 196.8075 (0.98‰) |
| | Mesh III | 77.7419 | 132.3057 | 132.3057 | 188.4393 | 196.8628 | 196.8628 (0.69‰) |
| | Ref. [71] | 77.79 | 132.3 | 132.3 | 188.6 | 197.0 | 197.0 (0‰) |
| | ABAQUS | 77.9299 | 132.7202 | 132.7202 | 189.1298 | 197.6068 | 197.6068 |
| 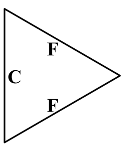 | Mesh I | 8.6418 | 31.3613 | 34.7885 | 75.3018 | 76.0219 | 86.9152 (1.20‰) |
| | Mesh II | 8.6433 | 31.3884 | 34.7981 | 75.3645 | 76.0880 | 86.9775 (0.49‰) |
| | Mesh III | 8.6438 | 31.3968 | 34.8010 | 75.3841 | 76.1084 | 86.9971 (0.26‰) |
| | Ref. [71] | 8.646 | 31.41 | 34.81 | 75.40 | 76.15 | 87.02 (0.00‰) |
| | ABAQUS | 8.6460 | 31.4342 | 34.8360 | 75.5201 | 76.2471 | 87.1583 |

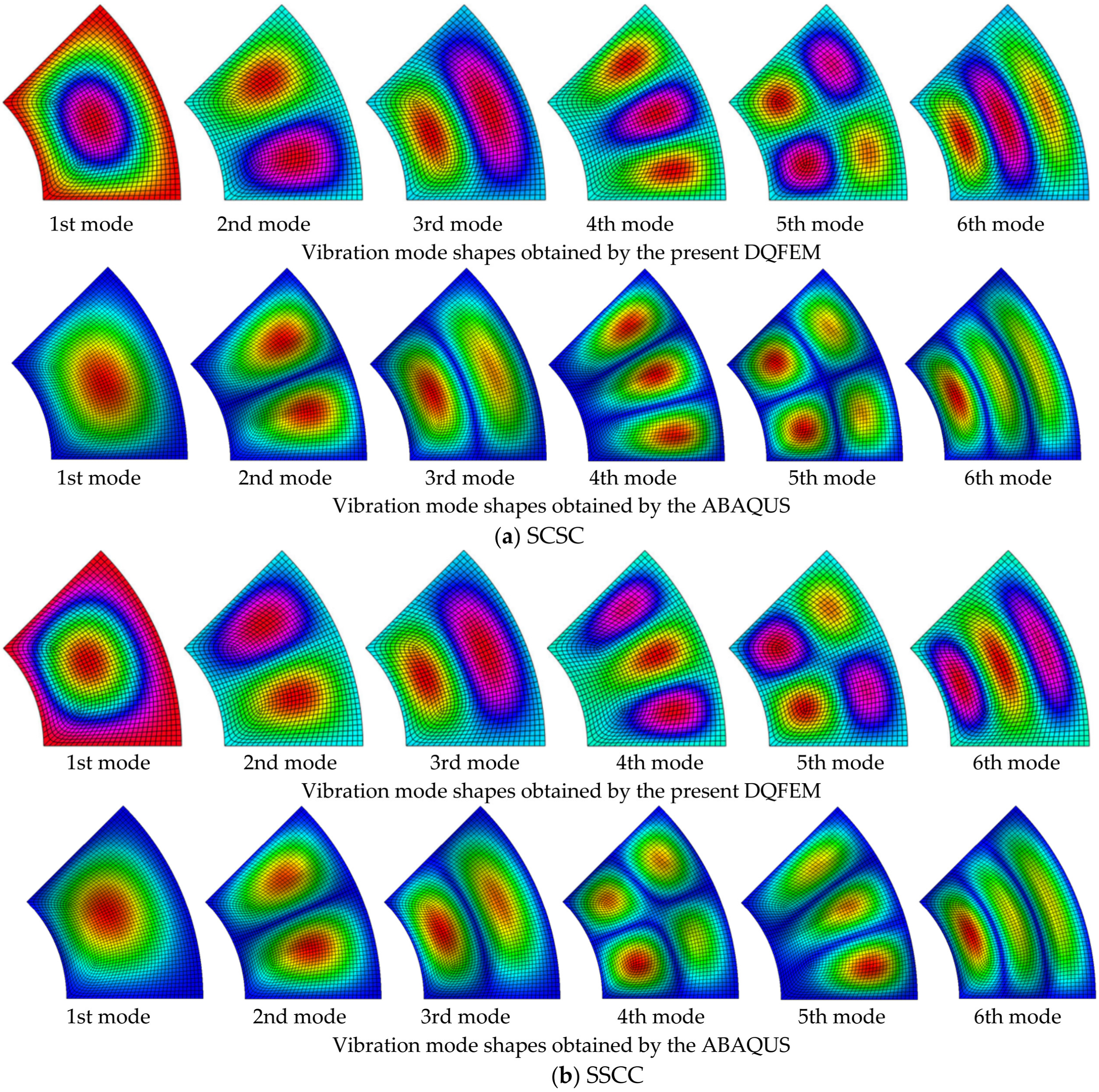


**Figure 5.** The six lowest vibration mode shapes of an annular sectorial Mindlin macroplate under three different boundary conditions (single attribute).

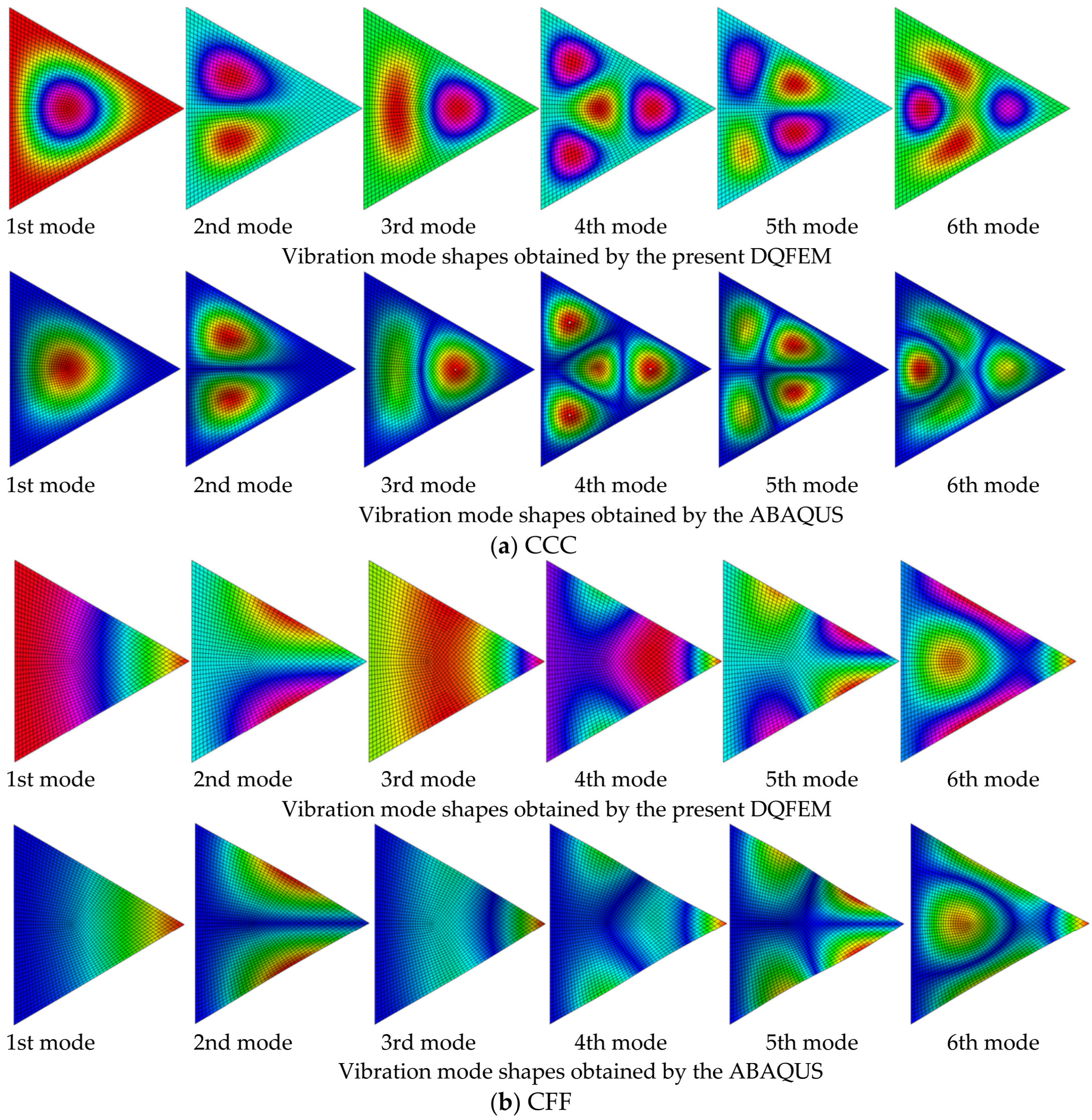


**Figure 6.** The six lowest vibration mode shapes of an equilateral triangular Mindlin macroplate under three different boundary conditions (single attribute).

Table 3 presents the eight lowest dimensionless frequencies of a square epoxy resin microplate with $L/h = 10$, E $= 1.44$ GPa, $\rho = 1220$ kg/m$^3$, $\nu = 0.38$, $l_s/h = 1$, and $l_d/h = 1$. It is noted that numerical and analytical frequencies can achieve consistency with the increase in the mesh density.

**Table 3.** The eight lowest dimensionless frequencies for a simply supported square microplate with different mesh densities (single attribute).

| Mode | Mesh Density | | | | | | Navier Method |
|---|---|---|---|---|---|---|---|
| | **4×4** | **8×8** | **12×12** | **16×16** | **20×20** | **24×24** | |
| $\overline{\omega}_1$ | 1.7737 | 1.7747 | 1.7747 | 1.7747 | 1.7747 | 1.7747 | 1.7747 |
| $\overline{\omega}_2$ | 3.9638 | 3.9502 | 3.9488 | 3.9485 | 3.9485 | 3.9484 | 3.9484 |
| $\overline{\omega}_3$ | 6.0028 | 5.9862 | 5.9839 | 5.9833 | 5.9831 | 5.9830 | 5.9830 |
| $\overline{\omega}_4$ | 7.1447 | 7.0213 | 7.0113 | 7.0094 | 7.0088 | 7.0086 | 7.0085 |
| $\overline{\omega}_5$ | 9.0701 | 8.9722 | 8.9628 | 8.9607 | 8.9601 | 8.9598 | 8.9595 |
| $\overline{\omega}_6$ | 11.7753 | 10.8629 | 10.8185 | 10.8101 | 10.8077 | 10.8068 | 10.8063 |
| $\overline{\omega}_7$ | 12.0071 | 11.8812 | 11.8680 | 11.8649 | 11.8638 | 11.8634 | 11.8630 |
| $\overline{\omega}_8$ | 13.5871 | 12.7407 | 12.7007 | 12.6928 | 12.6904 | 12.6895 | 12.6883 |

The variations in the logarithms of the 1-norms of reduced stiffness and mass matrices (after imposing essential boundary conditions) against strain gradient and inertia gradient parameters are illustrated in Figures 7 and 8, respectively. With the increase in gradient parameters, $\log_{10}(\mathrm{Cond}(\boldsymbol{K},\ 1))$ and $\log_{10}(\mathrm{Cond}(\boldsymbol{M},\ 1))$ both decrease. The flattened curves (see Figures 7 and 8) indicate that the increasing gradient parameters can improve the convergence of the elements.

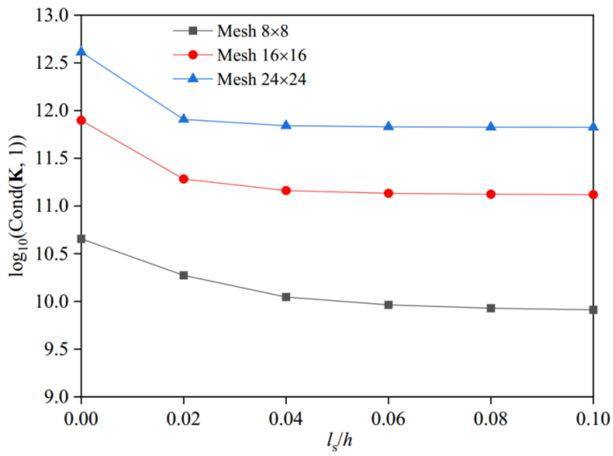


**Figure 7.** The logarithm of the 1-norm of reduced stiffness matrix varying with strain gradient parameter (single attribute).

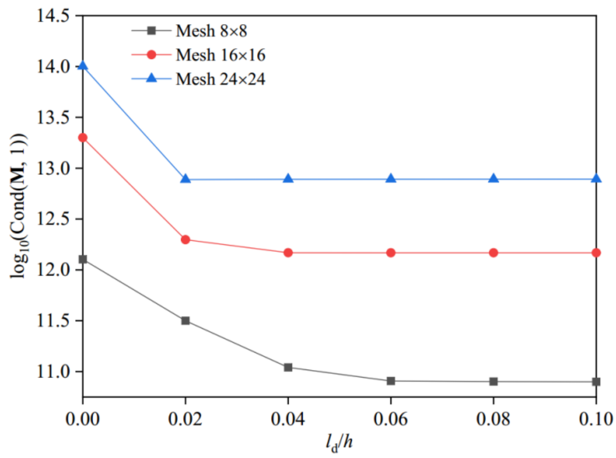


**Figure 8.** The logarithm of the 1-norm of reduced mass matrix varying with inertia gradient parameter (single attribute).

Table 4 lists the dimensionless fundamental frequencies presented by the present gradient elastic Mindlin plate model and the available gradient elastic Kirchhoff plate model in [68]. For comparison, the plate dimensions are $h = 0.34$ nm and $L_X = L_Y = 10$ nm. It can be seen that the present predictions are consistent with those in the literature when the plate is very thin.

**Table 4.** Comparison of dimensionless fundamental frequency for a square nanoplate with different gradient parameters (single attribute).

| Plate Type | $l_d$ | $l_s$ 0.2 nm Ref. [68] | $l_s$ 0.2 nm Present | $l_s$ 1.0 nm Ref. [68] | $l_s$ 1.0 nm Present |
|---|---|---|---|---|---|
| SFSF | 0.0 nm | 0.9774 | 0.9802 | 0.9878 | 0.9920 |
| | 0.2 nm | 0.9735 | 0.9761 | 0.9839 | 0.9864 |
| | 0.5 nm | 0.9539 | 0.9553 | 0.9640 | 0.9688 |
| | 1.0 nm | 0.8922 | 0.8945 | 0.9017 | 0.9079 |
| SCSF | 0.0 nm | 3.6907 | 3.6967 | 4.6619 | 4.6668 |
| | 0.2 nm | 3.6556 | 3.6620 | 4.6160 | 4.6198 |
| | 0.5 nm | 3.4858 | 3.4887 | 4.3949 | 4.3968 |
| | 1.0 nm | 3.0268 | 3.0302 | 3.8032 | 3.8046 |

### *4.2. Parameter Settings*

The solution method is then used to analyze the free vibration of gradient elastic annular sectorial and triangular microplates made of epoxy resin. Here, the material property parameters are assumed as [31] $E$= 1.44GPa, $\rho = 1220\text{kg/m}^2$, $K_s = 5/6$, and $\nu = 0.38$.

Tables 5 and 6 summarize the six lowest dimensionless frequencies for an annular sectorial microplate and an equilateral triangular microplate, where $\bar{l}_s = l_s/h$, $\bar{l}_d = l_d/h$, $R_{\text{out}}/h = 10$, and $L/h = 10$, and the underlined values in Table 5 are the ratios of the frequency for the case of $\bar{l}_s = 1$ (or $\bar{l}_d = 1$) to the frequency for the case of $\bar{l}_s = \bar{l}_d = 0$. As expected, an increased $\bar{l}_s$ or a decreased $\bar{l}_d$ can lead to the increasing vibration frequencies of microplates, especially for the higher-order modes. This is because the strain gradient and inertia gradient play roles in enhancing the structural bending rigidity and inertia. By comparing the underlined values in Table 6, we observe that strain gradient and inertia gradient effects become significant when increasing the order of the vibration mode, but they are slightly affected by the boundary conditions. However, variations in the frequency ratio against the order of the vibration mode are different between equilateral triangular and annular sectorial microplates. In Tables 5 and 6, the boundary condition has a more remarkable impact on the frequency ratio in the equilateral triangular case than it does in the annular sectorial case. By comparing the results shown in bold (Tables 5 and 6) between the cases of $\bar{l}_s = \bar{l}_d$= 0 and $\bar{l}_s = \bar{l}_d = 1$, we find that the inertia gradient has a greater influence on the frequencies than the strain gradient for the second vibration mode.

The six lowest vibration mode shapes of an annular sectorial microplate with SSCC edges and an equilateral triangular microplate with SCC edges are illustrated in Figures 9 and 10, respectively. In the figures, we observe that the first mode shape is almost unaffected by gradient parameters, while others are not. It is indicated that the introduced gradient effects change the vibration mode shapes, along with the frequency values. Similar observations have been previously reported in [57], where the authors show the four lowest eigenmodes of square and annular gradient elastic microplates with in-plane free vibrations.

**Table 5.** The six lowest dimensionless frequencies for an annular sectorial microplate with different boundary conditions and gradient parameters (single attribute).

| Plate Type | $(\bar{l}_s, \bar{l}_d)$ | Dimensionless Frequency | | | | | |
|---|---|---|---|---|---|---|---|
| | | $\bar{\omega}_1$ | $\bar{\omega}_2$ | $\bar{\omega}_3$ | $\bar{\omega}_4$ | $\bar{\omega}_5$ | $\bar{\omega}_6$ |
| 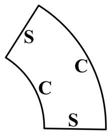  | **(0, 0)** | **81.5207** | **130.4961** | **168.5017** | **202.1629** | **211.4280** | **268.4294** |
| | (0.5, 0) | 95.3423 | 153.3994 | 207.0074 | 256.5577 | 272.0939 | 364.4674 |
| | (0, 0.5) | 72.2138 | 104.7030 | 131.3718 | 146.1192 | 152.6934 | 182.6297 |
| | (1, 0) | 124.5375 | 203.0303 | 281.0181 | 366.8073 | 393.5932 | 534.6659 |
| | | 1.5277 | 1.5558 | 1.6677 | 1.8144 | 1.8616 | 1.9918 |
| | (0, 1) | 55.9479 | 72.3129 | 88.2711 | 93.1260 | 97.2287 | 110.6023 |
| | | 0.6863 | 0.5541 | 0.5239 | 0.4606 | 0.4599 | 0.4120 |
| | **(1, 1)** | **87.4697** | **112.4565** | **143.7237** | **165.9530** | **178.1079** | **203.0451** |
| 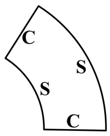  | **(0, 0)** | **74.2015** | **138.7872** | **149.6016** | **208.7868** | **211.5255** | **251.4064** |
| | (0.5, 0) | 86.4273 | 165.6917 | 178.8613 | 266.6957 | 273.2989 | 334.9031 |
| | (0, 0.5) | 65.5494 | 111.5257 | 116.0503 | 150.6620 | 153.5407 | 169.7088 |
| | (1, 0) | 111.5916 | 220.7434 | 239.4153 | 380.8189 | 393.0436 | 493.3882 |
| | | 1.5039 | 1.5905 | 1.6004 | 1.8240 | 1.8581 | 1.9625 |
| | (0, 1) | 50.6369 | 76.9966 | 77.9073 | 95.9221 | 98.1906 | 104.1261 |
| | | 0.6824 | 0.5548 | 0.5208 | 0.4642 | 0.4594 | 0.4142 |
| | **(1, 1)** | **76.1093** | **121.2415** | **125.4321** | **170.5555** | **175.3253** | **194.4725** |
| 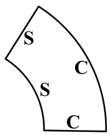  | **(0, 0)** | **79.2224** | **138.5925** | **161.0288** | **210.7184** | **212.4034** | **261.4489** |
| | (0.5, 0) | 93.0171 | 165.6100 | 195.9620 | 270.9050 | 275.0648 | 353.2054 |
| | (0, 0.5) | 69.8781 | 111.4121 | 125.3498 | 152.8662 | 153.3883 | 177.4652 |
| | (1, 0) | 122.1085 | 221.8823 | 266.1490 | 387.9548 | 399.3468 | 519.6088 |
| | | 1.5413 | 1.6010 | 1.6528 | 1.8411 | 1.8801 | 1.9874 |
| | (0, 1) | 53.7549 | 76.9914 | 84.3009 | 97.4848 | 97.8276 | 109.4238 |
| | | 0.6785 | 0.5555 | 0.5235 | 0.4626 | 0.4606 | 0.4185 |
| | **(1, 1)** | **84.5940** | **124.0212** | **138.3856** | **174.6448** | **181.5263** | **198.7258** |

**Table 6.** The six lowest dimensionless frequencies for an equilateral triangular microplate with different boundary conditions and gradient parameters (single attribute).

| Plate Type | $(\bar{l}_s, \bar{l}_d)$ | Dimensionless Frequency | | | | | |
|---|---|---|---|---|---|---|---|
| | | $\bar{\omega}_1$ | $\bar{\omega}_2$ | $\bar{\omega}_3$ | $\bar{\omega}_4$ | $\bar{\omega}_5$ | $\bar{\omega}_6$ |
| 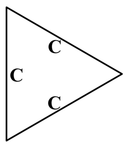  | **(0, 0)** | **76.2249** | **128.9764** | **128.9764** | **183.0821** | **191.1030** | **191.1030** |
| | (0.5, 0) | 84.1899 | 152.6676 | 152.6676 | 228.2820 | 238.8048 | 238.8048 |
| | (0, 0.5) | 68.9814 | 106.9641 | 106.9641 | 140.7625 | 143.9840 | 143.9840 |
| | (1, 0) | 101.3952 | 200.9779 | 200.9779 | 317.4252 | 331.8159 | 331.8159 |
| | | 1.3302 | 1.5583 | 1.5583 | 1.7338 | 1.7363 | 1.7363 |
| | (0, 1) | 55.0620 | 76.0369 | 76.0369 | 94.0234 | 94.1282 | 94.1282 |
| | | 0.7224 | 0.5895 | 0.5895 | 0.5136 | 0.4926 | 0.4926 |
| | **(1, 1)** | **75.4742** | **120.1357** | **120.6292** | **158.4080** | **158.7861** | **165.5730** |
| 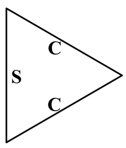  | **(0, 0)** | **66.3187** | **119.6351** | **119.8490** | **174.2392** | **183.0867** | **183.8417** |
| | (0.5, 0) | 72.0779 | 138.4393 | 140.1666 | 213.9839 | 225.1839 | 227.1890 |
| | (0, 0.5) | 59.7884 | 98.9798 | 99.1781 | 133.2975 | 137.7091 | 138.4922 |
| | (1, 0) | 84.7178 | 176.6627 | 182.8545 | 292.5272 | 308.8696 | 313.9850 |
| | | 1.2774 | 1.4767 | 1.5257 | 1.6789 | 1.6870 | 1.7079 |
| | (0, 1) | 47.5424 | 70.3561 | 70.5703 | 88.5408 | 90.0805 | 90.7414 |
| | | 0.7169 | 0.5881 | 0.5888 | 0.5082 | 0.4920 | 0.4936 |
| | **(1, 1)** | **61.6449** | **104.5859** | **108.3691** | **147.1023** | **148.1694** | **153.0898** |
| 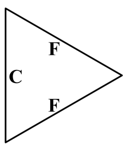  | **(0, 0)** | **8.4766** | **30.0886** | **33.8771** | **72.8753** | **73.1805** | **85.1658** |
| | (0.5, 0) | 11.6780 | 32.8524 | 38.9259 | 84.5572 | 84.8922 | 94.7538 |
| | (0, 0.5) | 8.2626 | 25.6136 | 30.7860 | 56.8479 | 60.8161 | 67.2185 |
| | (1, 0) | 16.5950 | 37.9233 | 48.0417 | 104.3431 | 105.8601 | 114.3535 |
| | | 1.9577 | 1.2604 | 1.4181 | 1.4318 | 1.4466 | 1.3427 |
| | (0, 1) | 7.7009 | 18.7560 | 24.9306 | 38.7446 | 42.6922 | 46.7500 |
| | | 0.9085 | 0.6234 | 0.7359 | 0.5317 | 0.5834 | 0.5489 |
| | **(1, 1)** | **15.2310** | **23.1984** | **34.8584** | **54.2883** | **55.8119** | **67.2840** |

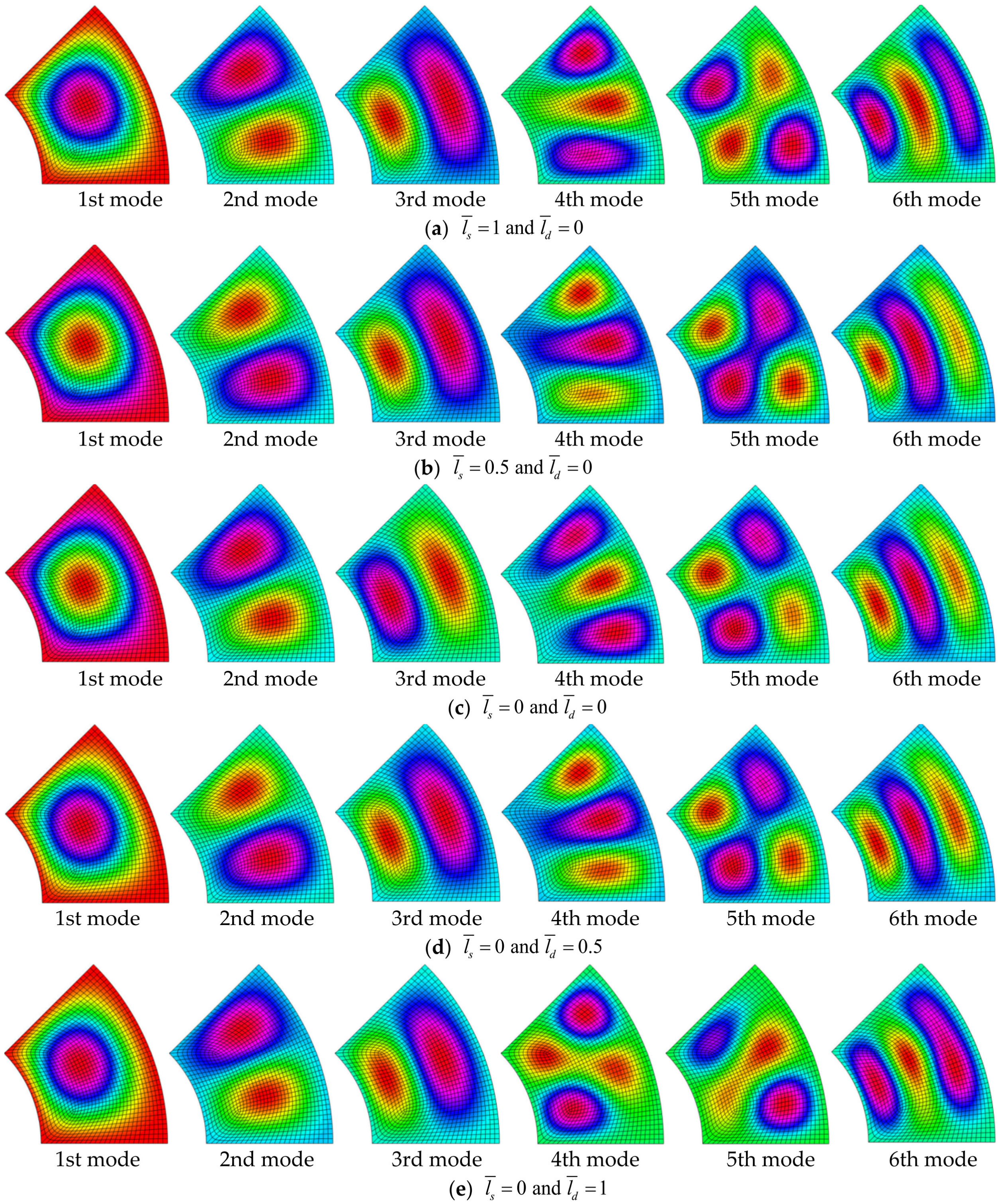


**Figure 9.** Two types of gradient effects on the six lowest vibration mode shapes of an annular sectorial microplate with SSCC edges (single attribute).

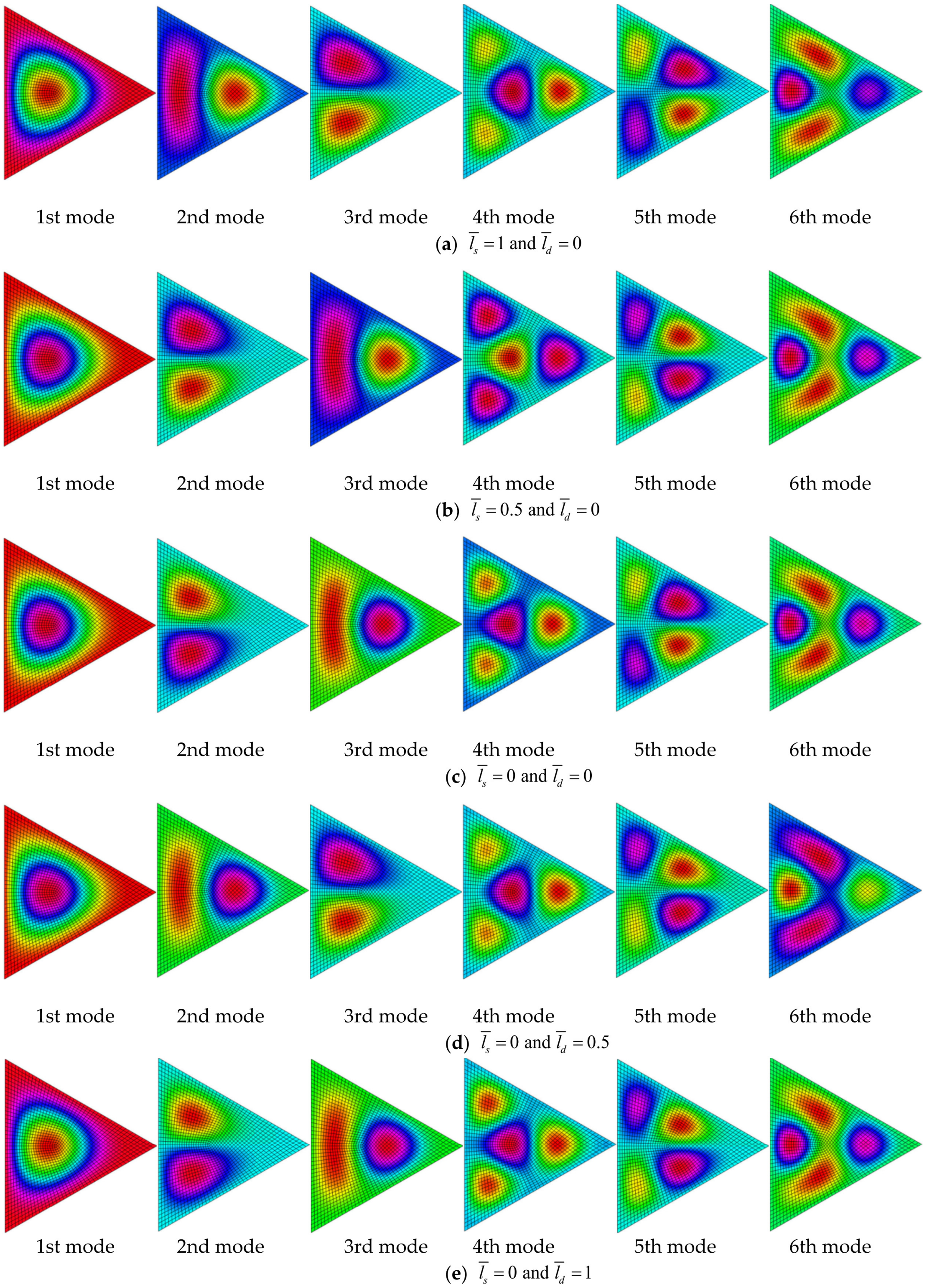


**Figure 10.** Two types of gradient effects on the six lowest vibration mode shapes of an equilateral triangular microplate with SCC edges (single attribute).

Figure 11 presents the 7th to 12th vibration mode shapes and the related frequencies of an annular sectorial microplate in terms of two outer radius-to-thickness ratios and two sets of gradient parameters, respectively. A comparison between Cases 1 and 3 (or Cases 2 and 4) shows that the transverse shear deformation can considerably change the higher-order vibration frequencies and mode shapes. The comprehensive effect of the strain gradient and inertia gradient causes a decrease in the vibration frequencies of the thick microplate.

Moreover, the size dependence of vibration mode shapes is also shown by comparing Case 1 with Case 2 (or Case 3 with 4).

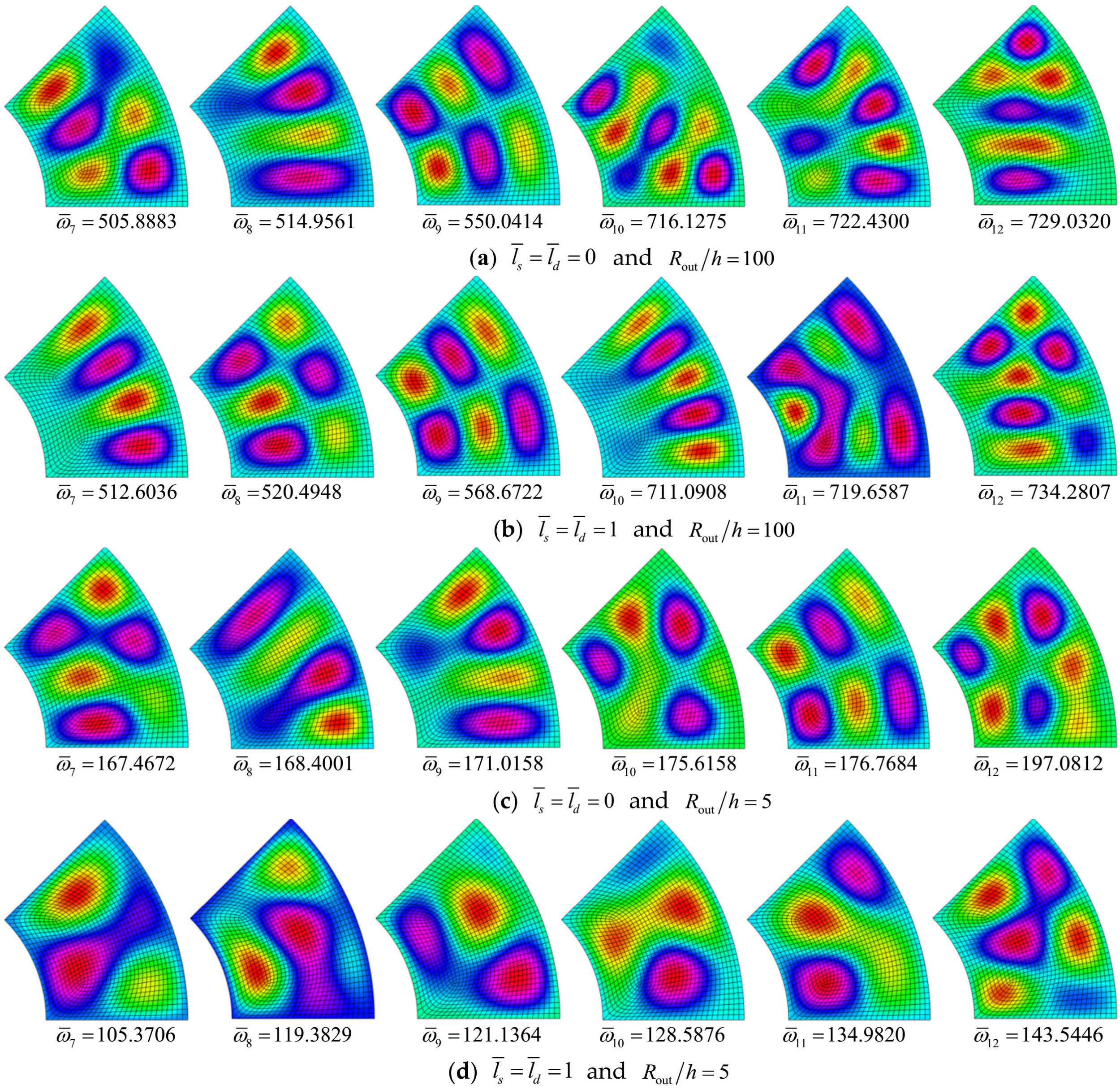


**Figure 11.** Transverse shear deformation effect on the 7th to 12th vibration frequencies and mode shapes of an annular sectorial microplate with SSCC edges (single attribute).

In addition, another comparative test has been conducted to confirm whether the normal curvature has an influence on the vibration mode shapes of an annular sectorial microplate with SSCC edges. As shown in Figure 12, considering the normal curvature, there are significant changes in the vibration mode shapes and increasing vibrational frequencies, especially for higher-order modes.

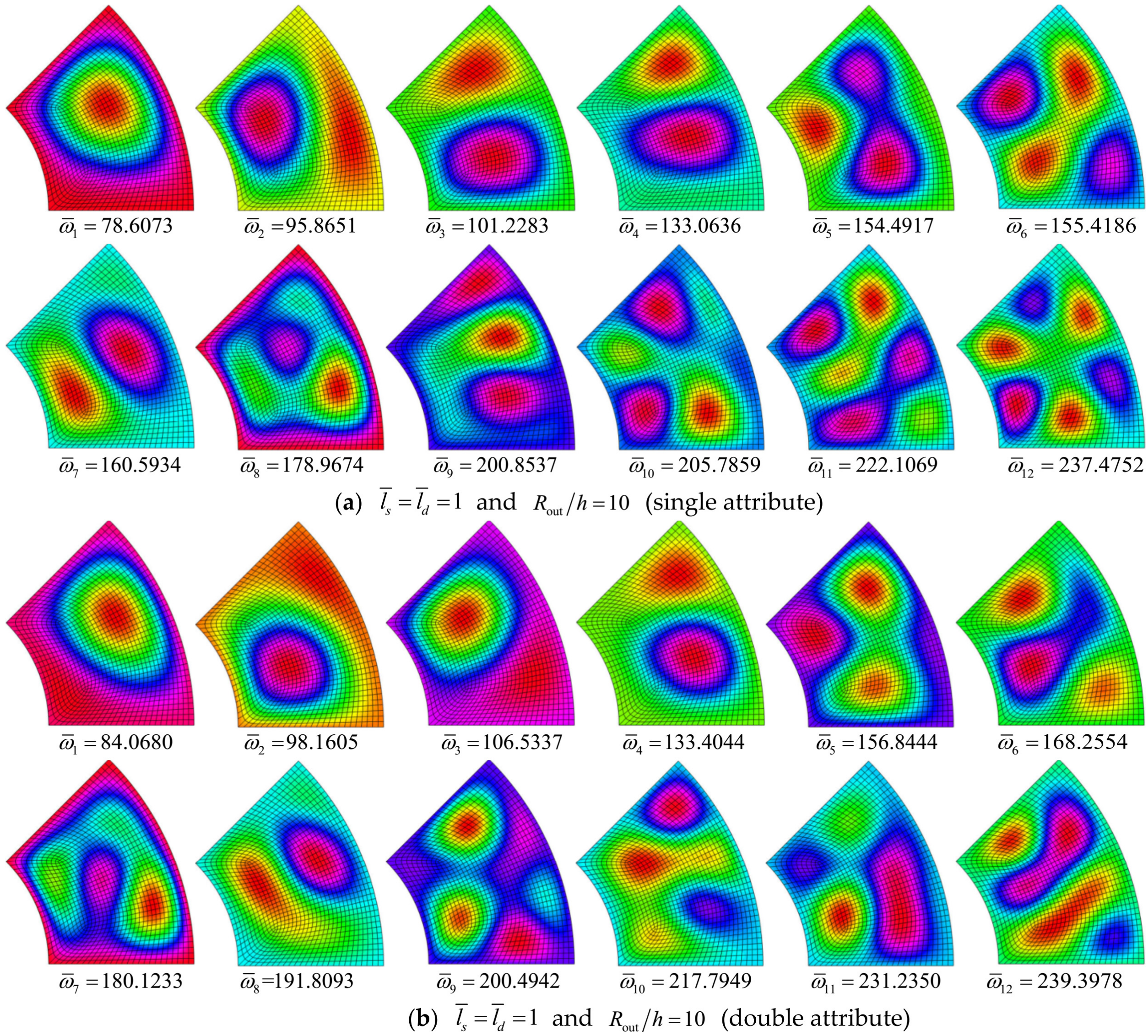


**Figure 12.** The normal curvature on the twelve lowest vibration frequencies and mode shapes of an annular sectorial microplate with SSCC edges.

## 5. Conclusions

In this article, we formulate the equations of motion and appropriate boundary conditions for Mindlin microplates with arbitrary shapes based on the negative second-order gradient elastic theory and the energy variational principle. A $C^1$-type four-node DQFE is proposed to analyze the resulting higher-order boundary value problems. Then, the DQ rule is properly used to convert the equation from natural coordinates into Cartesian coordinate systems in the straight-sided quadrilateral domain. The element stiffness matrix, mass matrix, and load vector are derived using the minimum-potential-energy principle. The effectiveness of our theoretical model and solution method is demonstrated in comparison to other methods. Finally, the free vibration of annular sectorial and triangular microplates is analyzed using the new solution method. Several interesting points are observed as follows.

(1) The element convergence can be improved by increasing two types of gradient effects.

(2) The strain gradient and inertia gradient can cause the frequency stiffening and softening effects of microplates, respectively.

(3) The vibration mode shapes can be changed to a certain extent by introducing two types of gradient effects.

(4) The high-order vibration frequencies and mode shapes are more sensitive to boundary conditions, transverse shear deformation, and gradient parameters.

**Author Contributions:** Conceptualization, B.Z. and F.X.; methodology, B.Z.; software, B.Z.; validation, B.Z., L.Z. and C.L.; formal analysis, F.X.; investigation, F.X.; resources, C.L.; data curation, B.Z.; writing—original draft preparation, B.Z.; writing—review and editing, F.X.; visualization, B.Z.; supervision, C.L.; project administration, C.L.; funding acquisition, C.L. All authors have read and agreed to the published version of the manuscript.

**Funding:** This research was funded by the National Natural Science Foundation of China with grant number 11602204, the Fundamental Research Funds for the Central Universities of China with grant number 2682022ZTPY081, the Open Project of Applied Mechanics and Structure Safety Key Laboratory of Sichuan Province with grant number SZDKF-202102, and the National Natural Science Foundation of Sichuan Province with grant number 23NSFSC0849.

**Data Availability Statement:** Not applicable.

**Conflicts of Interest:** The authors declare no conflict of interest.

## Appendix A

The coordinate-transformation-related coefficients $\beta_{\mathrm{m}}$ are as follows:

$$
\begin{aligned}
\beta_1 &= \Gamma_5\left[\left(\frac{\partial\overline{X}}{\partial X}\right)^2+\left(\frac{\partial\overline{X}}{\partial Y}\right)^2\right]^2,\\
\beta_3 &= 4\Gamma_5\left[\left(\frac{\partial\overline{X}}{\partial Y}\right)^2\left(\frac{\partial\overline{Y}}{\partial Y}\right)^2+\left(\frac{\partial\overline{X}}{\partial X}\right)^2\left(\frac{\partial\overline{Y}}{\partial X}\right)^2\right]+2\Gamma_5\left(\frac{\partial\overline{Y}}{\partial X}\frac{\partial\overline{X}}{\partial Y}+\frac{\partial\overline{X}}{\partial X}\frac{\partial\overline{Y}}{\partial Y}\right)^2,\\
\beta_2 &= \Gamma_5\left[\left(\frac{\partial\overline{Y}}{\partial X}\right)^2+\left(\frac{\partial\overline{Y}}{\partial Y}\right)^2\right]^2,\ \beta_4 = 2\Gamma_5\left(\frac{\partial\overline{X}}{\partial X}\frac{\partial\overline{Y}}{\partial X}+\frac{\partial\overline{X}}{\partial Y}\frac{\partial\overline{Y}}{\partial Y}\right)^2,\\
\beta_5 &= 4\,\Gamma_5\left[\left(\frac{\partial\overline{X}}{\partial X}\right)^2+\left(\frac{\partial\overline{X}}{\partial Y}\right)^2\right]\left(\frac{\partial\overline{X}}{\partial X}\frac{\partial\overline{Y}}{\partial X}+\frac{\partial\overline{X}}{\partial Y}\frac{\partial\overline{Y}}{\partial Y}\right),\\
\beta_6 &= 4\,\Gamma_5\left[\left(\frac{\partial\overline{Y}}{\partial X}\right)^2+\left(\frac{\partial\overline{Y}}{\partial Y}\right)^2\right]\left(\frac{\partial\overline{X}}{\partial X}\frac{\partial\overline{Y}}{\partial X}+\frac{\partial\overline{X}}{\partial Y}\frac{\partial\overline{Y}}{\partial Y}\right),\\
\beta_7 &= \left[\left(\frac{\partial\overline{X}}{\partial X}\right)^2+\left(\frac{\partial\overline{X}}{\partial Y}\right)^2\right]\left[\Gamma_7\left(\frac{\partial\overline{X}}{\partial X}\right)^2+\Gamma_6\left(\frac{\partial\overline{X}}{\partial Y}\right)^2\right],\\
\beta_8 &= \left[\left(\frac{\partial\overline{Y}}{\partial X}\right)^2+\left(\frac{\partial\overline{Y}}{\partial Y}\right)^2\right]\left[\Gamma_7\left(\frac{\partial\overline{Y}}{\partial X}\right)^2+\Gamma_6\left(\frac{\partial\overline{Y}}{\partial Y}\right)^2\right],\\
\beta_{10} &= 2\,\left(\frac{\partial\overline{X}}{\partial X}\frac{\partial\overline{Y}}{\partial X}+\frac{\partial\overline{X}}{\partial Y}\frac{\partial\overline{Y}}{\partial Y}\right)\left(\Gamma_7\frac{\partial\overline{X}}{\partial X}\frac{\partial\overline{Y}}{\partial X}+\Gamma_6\frac{\partial\overline{X}}{\partial Y}\frac{\partial\overline{Y}}{\partial Y}\right),\\
\beta_9 &= 4\,\Gamma_7\left(\frac{\partial\overline{X}}{\partial X}\right)^2\left(\frac{\partial\overline{Y}}{\partial X}\right)^2+4\Gamma_6\left(\frac{\partial\overline{X}}{\partial Y}\right)^2\left(\frac{\partial\overline{Y}}{\partial Y}\right)^2+(\Gamma_7+\Gamma_6)\left(\frac{\partial\overline{Y}}{\partial X}\frac{\partial\overline{X}}{\partial Y}+\frac{\partial\overline{X}}{\partial X}\frac{\partial\overline{Y}}{\partial Y}\right)^2,\\
\beta_{11} &= 2\,(\Gamma_6+\Gamma_7)\frac{\partial\overline{X}}{\partial X}\frac{\partial\overline{X}}{\partial Y}\left(\frac{\partial\overline{Y}}{\partial X}\frac{\partial\overline{X}}{\partial Y}+\frac{\partial\overline{X}}{\partial X}\frac{\partial\overline{Y}}{\partial Y}\right)+4\,\Gamma_7\left(\frac{\partial\overline{X}}{\partial X}\right)^3\frac{\partial\overline{Y}}{\partial X}+4\,\Gamma_6\left(\frac{\partial\overline{X}}{\partial Y}\right)^3\frac{\partial\overline{Y}}{\partial Y},\\
\beta_{12} &= 2\,(\Gamma_6+\Gamma_7)\frac{\partial\overline{Y}}{\partial X}\frac{\partial\overline{Y}}{\partial Y}\left(\frac{\partial\overline{Y}}{\partial X}\frac{\partial\overline{X}}{\partial Y}+\frac{\partial\overline{X}}{\partial X}\frac{\partial\overline{Y}}{\partial Y}\right)+4\,\Gamma_7\left(\frac{\partial\overline{Y}}{\partial X}\right)^3\frac{\partial\overline{X}}{\partial X}+4\,\Gamma_6\left(\frac{\partial\overline{Y}}{\partial Y}\right)^3\frac{\partial\overline{X}}{\partial Y},\\
\beta_{13} &= \left[\left(\frac{\partial\overline{X}}{\partial X}\right)^2+\left(\frac{\partial\overline{X}}{\partial Y}\right)^2\right]\left[\Gamma_6\left(\frac{\partial\overline{X}}{\partial X}\right)^2+\Gamma_7\left(\frac{\partial\overline{X}}{\partial Y}\right)^2\right],\\
\beta_{14} &= \left[\left(\frac{\partial\overline{Y}}{\partial X}\right)^2+\left(\frac{\partial\overline{Y}}{\partial Y}\right)^2\right]\left[\Gamma_6\left(\frac{\partial\overline{Y}}{\partial X}\right)^2+\Gamma_7\left(\frac{\partial\overline{Y}}{\partial Y}\right)^2\right],\\
\beta_{15} &= (\Gamma_6+\Gamma_7)\left(\frac{\partial\overline{X}}{\partial Y}\frac{\partial\overline{Y}}{\partial X}+\frac{\partial\overline{X}}{\partial X}\frac{\partial\overline{Y}}{\partial Y}\right)^2+4\,\Gamma_7\left(\frac{\partial\overline{X}}{\partial Y}\right)^2\left(\frac{\partial\overline{Y}}{\partial Y}\right)^2+4\,\Gamma_6\left(\frac{\partial\overline{X}}{\partial X}\right)^2\left(\frac{\partial\overline{Y}}{\partial X}\right)^2,\\
\beta_{16} &= 2\,\left(\frac{\partial\overline{X}}{\partial X}\frac{\partial\overline{Y}}{\partial X}+\frac{\partial\overline{X}}{\partial Y}\frac{\partial\overline{Y}}{\partial Y}\right)\left(\Gamma_6\frac{\partial\overline{X}}{\partial X}\frac{\partial\overline{Y}}{\partial X}+\Gamma_7\frac{\partial\overline{X}}{\partial Y}\frac{\partial\overline{Y}}{\partial Y}\right),\\
\beta_{19} &= (2\,\Gamma_6+\Gamma_8)\frac{\partial\overline{X}}{\partial X}\frac{\partial\overline{X}}{\partial Y}\left[\left(\frac{\partial\overline{X}}{\partial X}\right)^2+\left(\frac{\partial\overline{X}}{\partial Y}\right)^2\right],\\
\beta_{17} &= 2\,(\Gamma_6+\Gamma_7)\frac{\partial\overline{X}}{\partial X}\frac{\partial\overline{X}}{\partial Y}\left(\frac{\partial\overline{Y}}{\partial X}\frac{\partial\overline{X}}{\partial Y}+\frac{\partial\overline{X}}{\partial Y}\frac{\partial\overline{Y}}{\partial Y}\right)+4\,\Gamma_7\left(\frac{\partial\overline{X}}{\partial Y}\right)^3\frac{\partial\overline{Y}}{\partial Y}+4\,\Gamma_6\left(\frac{\partial\overline{X}}{\partial X}\right)^3\frac{\partial\overline{Y}}{\partial X},\\
\beta_{18} &= 2\,(\Gamma_6+\Gamma_7)\frac{\partial\overline{Y}}{\partial X}\frac{\partial\overline{Y}}{\partial Y}\left(\frac{\partial\overline{Y}}{\partial X}\frac{\partial\overline{X}}{\partial Y}+\frac{\partial\overline{X}}{\partial X}\frac{\partial\overline{Y}}{\partial Y}\right)+4\,\Gamma_7\left(\frac{\partial\overline{Y}}{\partial Y}\right)^3\frac{\partial\overline{X}}{\partial Y}+4\,\Gamma_6\left(\frac{\partial\overline{Y}}{\partial X}\right)^3\frac{\partial\overline{X}}{\partial X},\\
\beta_{20} &= (2\,\Gamma_6+\Gamma_8)\frac{\partial\overline{Y}}{\partial X}\frac{\partial\overline{Y}}{\partial Y}\left[\left(\frac{\partial\overline{Y}}{\partial X}\right)^2+\left(\frac{\partial\overline{Y}}{\partial Y}\right)^2\right],
\end{aligned}
\tag{A1}
$$

$$
\begin{aligned}
\beta_{21} &= \left(\frac{\partial \overline{X}}{\partial X}\frac{\partial \overline{Y}}{\partial X} + \frac{\partial \overline{X}}{\partial Y}\frac{\partial \overline{Y}}{\partial Y}\right)\left(\Gamma_8 \frac{\partial \overline{X}}{\partial X}\frac{\partial \overline{Y}}{\partial Y} + 2\,\Gamma_6 \frac{\partial \overline{Y}}{\partial X}\frac{\partial \overline{X}}{\partial Y}\right),\\
\beta_{22} &= \left(\frac{\partial \overline{X}}{\partial X}\frac{\partial \overline{Y}}{\partial X} + \frac{\partial \overline{X}}{\partial Y}\frac{\partial \overline{Y}}{\partial Y}\right)\left(2\Gamma_6 \frac{\partial \overline{X}}{\partial X}\frac{\partial \overline{Y}}{\partial Y} + \Gamma_8 \frac{\partial \overline{Y}}{\partial X}\frac{\partial \overline{X}}{\partial Y}\right),\\
\beta_{23} &= \Gamma_8 \frac{\partial \overline{X}}{\partial X}\left[\left(\frac{\partial \overline{X}}{\partial X}\right)^2 \frac{\partial \overline{Y}}{\partial Y} + \frac{\partial \overline{X}}{\partial X}\frac{\partial \overline{Y}}{\partial X}\frac{\partial \overline{X}}{\partial Y} + 2\left(\frac{\partial \overline{X}}{\partial Y}\right)^2 \frac{\partial \overline{Y}}{\partial Y}\right] +\\
&\quad 2\Gamma_6 \frac{\partial \overline{X}}{\partial Y}\left[2\left(\frac{\partial \overline{X}}{\partial X}\right)^2 \frac{\partial \overline{Y}}{\partial X} + \frac{\partial \overline{X}}{\partial X}\frac{\partial \overline{X}}{\partial Y}\frac{\partial \overline{Y}}{\partial Y} + \frac{\partial \overline{Y}}{\partial X}\left(\frac{\partial \overline{X}}{\partial Y}\right)^2\right],\\
\beta_{24} &= \Gamma_8 \frac{\partial \overline{Y}}{\partial X}\left[\frac{\partial \overline{X}}{\partial X}\frac{\partial \overline{Y}}{\partial X}\frac{\partial \overline{Y}}{\partial Y} + \left(\frac{\partial \overline{Y}}{\partial X}\right)^2 \frac{\partial \overline{X}}{\partial Y} + 2\,\frac{\partial \overline{X}}{\partial Y}\left(\frac{\partial \overline{Y}}{\partial Y}\right)^2\right] +\\
&\quad 2\,\Gamma_6 \frac{\partial \overline{Y}}{\partial Y}\left[2\,\frac{\partial \overline{X}}{\partial X}\left(\frac{\partial \overline{Y}}{\partial X}\right)^2 + \frac{\partial \overline{X}}{\partial X}\left(\frac{\partial \overline{Y}}{\partial Y}\right)^2 + \frac{\partial \overline{Y}}{\partial X}\frac{\partial \overline{X}}{\partial Y}\frac{\partial \overline{Y}}{\partial Y}\right],\\
\beta_{25} &= \Gamma_8 \frac{\partial \overline{Y}}{\partial Y}\left[2\,\frac{\partial \overline{X}}{\partial X}\left(\frac{\partial \overline{Y}}{\partial X}\right)^2 + \frac{\partial \overline{X}}{\partial X}\left(\frac{\partial \overline{Y}}{\partial Y}\right)^2 + \frac{\partial \overline{Y}}{\partial X}\frac{\partial \overline{X}}{\partial Y}\frac{\partial \overline{Y}}{\partial Y}\right] +\\
&\quad 2\Gamma_6 \frac{\partial \overline{Y}}{\partial X}\left[\frac{\partial \overline{X}}{\partial X}\frac{\partial \overline{Y}}{\partial X}\frac{\partial \overline{Y}}{\partial Y} + \left(\frac{\partial \overline{Y}}{\partial X}\right)^2 \frac{\partial \overline{X}}{\partial Y} + 2\,\frac{\partial \overline{X}}{\partial Y}\left(\frac{\partial \overline{Y}}{\partial Y}\right)^2\right],\\
\beta_{26} &= \Gamma_8 \frac{\partial \overline{X}}{\partial Y}\left[2\left(\frac{\partial \overline{X}}{\partial X}\right)^2 \frac{\partial \overline{Y}}{\partial X} + \frac{\partial \overline{X}}{\partial X}\frac{\partial \overline{X}}{\partial Y}\frac{\partial \overline{Y}}{\partial Y} + \frac{\partial \overline{Y}}{\partial X}\left(\frac{\partial \overline{X}}{\partial Y}\right)^2\right] +\\
&\quad 2\Gamma_6 \frac{\partial \overline{X}}{\partial X}\left[\left(\frac{\partial \overline{X}}{\partial X}\right)^2 \frac{\partial \overline{Y}}{\partial Y} + \frac{\partial \overline{X}}{\partial X}\frac{\partial \overline{Y}}{\partial X}\frac{\partial \overline{X}}{\partial Y} + 2\left(\frac{\partial \overline{X}}{\partial Y}\right)^2 \frac{\partial \overline{Y}}{\partial Y}\right],\\
\beta_{27} &= 2\,(2\,\Gamma_6 + \Gamma_8)\left(\frac{\partial \overline{Y}}{\partial X}\frac{\partial \overline{X}}{\partial Y} + \frac{\partial \overline{X}}{\partial X}\frac{\partial \overline{Y}}{\partial Y}\right)\left(\frac{\partial \overline{X}}{\partial X}\frac{\partial \overline{Y}}{\partial X} + \frac{\partial \overline{X}}{\partial Y}\frac{\partial \overline{Y}}{\partial Y}\right),\ \beta_{28} = 2\Gamma_5 \frac{\partial \overline{Y}}{\partial X}\left[\left(\frac{\partial \overline{Y}}{\partial X}\right)^2 + \left(\frac{\partial \overline{Y}}{\partial Y}\right)^2\right],\\
\beta_{29} &= 2\Gamma_5 \frac{\partial \overline{Y}}{\partial X}\left(\frac{\partial \overline{X}}{\partial X}\frac{\partial \overline{Y}}{\partial X} + \frac{\partial \overline{X}}{\partial Y}\frac{\partial \overline{Y}}{\partial Y}\right),\ \beta_{30} = 2\,\Gamma_5 \frac{\partial \overline{Y}}{\partial Y}\left[\left(\frac{\partial \overline{Y}}{\partial X}\right)^2 + \left(\frac{\partial \overline{Y}}{\partial Y}\right)^2\right],\\
\beta_{31} &= 2\,\Gamma_5 \frac{\partial \overline{Y}}{\partial Y}\left(\frac{\partial \overline{X}}{\partial X}\frac{\partial \overline{Y}}{\partial X} + \frac{\partial \overline{X}}{\partial Y}\frac{\partial \overline{Y}}{\partial Y}\right), \beta_{32} = 2\Gamma_5 \frac{\partial \overline{X}}{\partial X}\left(\frac{\partial \overline{X}}{\partial X}\frac{\partial \overline{Y}}{\partial X} + \frac{\partial \overline{X}}{\partial Y}\frac{\partial \overline{Y}}{\partial Y}\right),\\
\beta_{33} &= 2\Gamma_5\, \frac{\partial \overline{X}}{\partial X}\left[\left(\frac{\partial \overline{X}}{\partial X}\right)^2 + \left(\frac{\partial \overline{X}}{\partial Y}\right)^2\right],\ \beta_{34} = 2\,\Gamma_5 \frac{\partial \overline{X}}{\partial Y}\left(\frac{\partial \overline{X}}{\partial X}\frac{\partial \overline{Y}}{\partial X} + \frac{\partial \overline{X}}{\partial Y}\frac{\partial \overline{Y}}{\partial Y}\right),\\
\beta_{35} &= 2\Gamma_5\, \frac{\partial \overline{X}}{\partial Y}\left[\left(\frac{\partial \overline{X}}{\partial X}\right)^2 + \left(\frac{\partial \overline{X}}{\partial Y}\right)^2\right],\ \beta_{36} = 2\Gamma_5\left[2\,\frac{\partial \overline{X}}{\partial X}\left(\frac{\partial \overline{Y}}{\partial X}\right)^2 + \frac{\partial \overline{X}}{\partial X}\left(\frac{\partial \overline{Y}}{\partial Y}\right)^2 + \frac{\partial \overline{Y}}{\partial X}\frac{\partial \overline{X}}{\partial Y}\frac{\partial \overline{Y}}{\partial Y}\right],\\
\beta_{40} &= (2\Gamma_2 + \Gamma_3)\frac{\partial \overline{Y}}{\partial X}\frac{\partial \overline{Y}}{\partial Y}, \beta_{37} = 2\,\Gamma_5\left[2\left(\frac{\partial \overline{X}}{\partial X}\right)^2 \frac{\partial \overline{Y}}{\partial X} + \frac{\partial \overline{X}}{\partial X}\frac{\partial \overline{X}}{\partial Y}\frac{\partial \overline{Y}}{\partial Y} + \frac{\partial \overline{Y}}{\partial X}\left(\frac{\partial \overline{X}}{\partial Y}\right)^2\right],\\
\beta_{41} &= 2\,\Gamma_2 \frac{\partial \overline{Y}}{\partial Y}\frac{\partial \overline{X}}{\partial X} + \Gamma_3 \frac{\partial \overline{Y}}{\partial X}\frac{\partial \overline{X}}{\partial Y}, \beta_{38} = 2\,\Gamma_5\left[\frac{\partial \overline{X}}{\partial X}\frac{\partial \overline{Y}}{\partial X}\frac{\partial \overline{Y}}{\partial Y} + \left(\frac{\partial \overline{Y}}{\partial X}\right)^2 \frac{\partial \overline{X}}{\partial Y} + 2\,\frac{\partial \overline{X}}{\partial Y}\left(\frac{\partial \overline{Y}}{\partial Y}\right)^2\right],\\
\beta_{42} &= 2\,(\Gamma_2 + \Gamma_5)\frac{\partial \overline{X}}{\partial Y}\frac{\partial \overline{Y}}{\partial Y} + 2(\Gamma_4 + \Gamma_5)\frac{\partial \overline{X}}{\partial X}\frac{\partial \overline{Y}}{\partial X},\\
\beta_{39} &= 2\,\Gamma_5\left[\left(\frac{\partial \overline{X}}{\partial X}\right)^2 \frac{\partial \overline{Y}}{\partial Y} + \frac{\partial \overline{X}}{\partial X}\frac{\partial \overline{Y}}{\partial X}\frac{\partial \overline{X}}{\partial Y} + 2\left(\frac{\partial \overline{X}}{\partial Y}\right)^2 \frac{\partial \overline{Y}}{\partial Y}\right],\\
\beta_{43} &= 2\Gamma_2 \frac{\partial \overline{X}}{\partial Y}\frac{\partial \overline{Y}}{\partial X} + \Gamma_3 \frac{\partial \overline{X}}{\partial X}\frac{\partial \overline{Y}}{\partial Y}, \beta_{44} = (2\Gamma_2 + \Gamma_3)\frac{\partial \overline{X}}{\partial X}\frac{\partial \overline{X}}{\partial Y},\\
\beta_{45} &= 2\,(\Gamma_4 + \Gamma_5)\frac{\partial \overline{X}}{\partial Y}\frac{\partial \overline{Y}}{\partial Y} + 2\,(\Gamma_2 + \Gamma_5)\frac{\partial \overline{X}}{\partial X}\frac{\partial \overline{Y}}{\partial X},\ \beta_{46} = \Gamma_1\left[\left(\frac{\partial \overline{X}}{\partial X}\right)^2 + \left(\frac{\partial \overline{X}}{\partial Y}\right)^2\right],\\
\beta_{47} &= \Gamma_1\left[\left(\frac{\partial \overline{Y}}{\partial X}\right)^2 + \left(\frac{\partial \overline{Y}}{\partial Y}\right)^2\right],\ \beta_{48} = (\Gamma_5 + \Gamma_4)\left(\frac{\partial \overline{X}}{\partial X}\right)^2 + (\Gamma_2 + \Gamma_5)\left(\frac{\partial \overline{X}}{\partial Y}\right)^2,\\
\beta_{49} &= (\Gamma_5 + \Gamma_4)\left(\frac{\partial \overline{Y}}{\partial X}\right)^2 + (\Gamma_5 + \Gamma_2)\left(\frac{\partial \overline{Y}}{\partial Y}\right)^2, \beta_{50} = (\Gamma_5 + \Gamma_2)\left(\frac{\partial \overline{X}}{\partial X}\right)^2 + (\Gamma_5 + \Gamma_4)\left(\frac{\partial \overline{X}}{\partial Y}\right)^2,\\
\beta_{51} &= (\Gamma_5 + \Gamma_4)\left(\frac{\partial \overline{Y}}{\partial Y}\right)^2 + (\Gamma_5 + \Gamma_2)\left(\frac{\partial \overline{Y}}{\partial X}\right)^2,\ \beta_{53} = 2\,\Gamma_1 \frac{\partial \overline{X}}{\partial X},\\
\beta_{52} &= 2\Gamma_1\left(\frac{\partial \overline{X}}{\partial X}\frac{\partial \overline{Y}}{\partial X} + \frac{\partial \overline{X}}{\partial Y}\frac{\partial \overline{Y}}{\partial Y}\right),\ \beta_{54} = 2\,\Gamma_1 \frac{\partial \overline{Y}}{\partial X},\ \beta_{55} = 2\,\Gamma_1 \frac{\partial \overline{X}}{\partial Y},\\
\beta_{56} &= 2\,\Gamma_1 \frac{\partial \overline{Y}}{\partial Y},\ \beta_{57} = \Gamma_1.
\end{aligned}
$$

## References


1. Bui, T.Q.; Doan, D.H.; Van Do, T.; Hirose, S.; Duc, N.D. High frequency modes meshfree analysis of Reissner–Mindlin plates. *J. Sci. Adv. Mater. Devices* **2016**, *1*, 400–412. [CrossRef]
2. Nam, V.H.; Nam, N.H.; Vinh, P.V.; Khoa, D.N.; Thom, D.V.; Minh, P.V. A New Efficient Modified First-Order Shear Model for Static Bending and Vibration Behaviors of Two-Layer Composite Plate. *Adv. Civ. Eng.* **2019**, *2019*, 6814367. [CrossRef]
3. Tran, T.T.; Nguyen, N.H.; Do, T.V.; Minh, P.V.; Duc, N.D. Bending and thermal buckling of unsymmetric functionally graded sandwich beams in high-temperature environment based on a new third-order shear deformation theory. *J. Sandw. Struct. Mater.* **2019**, *23*, 906–930. [CrossRef]
4. Thai, L.M.; Luat, D.T.; Phung, V.B.; Minh, P.V.; Thom, D.V. Finite element modeling of mechanical behaviors of piezoelectric nanoplates with flexoelectric effects. *Arch. Appl. Mech.* **2022**, *92*, 163–182. [CrossRef]
5. Doan, D.H.; Zenkour, A.M.; Van Thom, D. Finite element modeling of free vibration of cracked nanoplates with flexoelectric effects. *Eur. Phys. J. Plus* **2022**, *137*, 447. [CrossRef]
6. Duc, N.D.; Trinh, T.D.; Do, T.V.; Doan, D.H. On the buckling behavior of multi-cracked FGM plates. In Proceedings of the International Conference on Advances in Computational Mechanics, Phu Quoc Island, Vietnam, 2–4 August 2017; pp. 29–45.
7. Choudhary, V.; Iniewski, K. *Mems: Fundamental Technology and Applications*; CRC Press: Boca Raton, FL, USA, 2016.
8. Lam, D.C.; Yang, F.; Chong, A.; Wang, J.; Tong, P. Experiments and theory in strain gradient elasticity. *J. Mech. Phys. Solids* **2003**, *51*, 1477–1508. [CrossRef]
9. Lei, J.; He, Y.; Guo, S.; Li, Z.; Liu, D. Size-dependent vibration of nickel cantilever microbeams: Experiment and gradient elasticity. *AIP Adv.* **2016**, *6*, 105202. [CrossRef]
10. Li, Z.; He, Y.; Zhang, B.; Lei, J.; Guo, S.; Liu, D. Experimental investigation and theoretical modelling on nonlinear dynamics of cantilevered microbeams. *Eur. J. Mech. A/Solids* **2019**, *78*, 103834. [CrossRef]
11. Liu, D.; He, Y.; Tang, X.; Ding, H.; Hu, P.; Cao, P. Size effects in the torsion of microscale copper wires: Experiment and analysis. *Scr. Mater.* **2012**, *66*, 406–409. [CrossRef]
12. Polyzos, D.; Huber, G.; Mylonakis, G.; Triantafyllidis, T.; Papargyri-Beskou, S.; Beskos, D. Torsional vibrations of a column of fine-grained material: A gradient elastic approach. *J. Mech. Phys. Solids* **2015**, *76*, 338–358. [CrossRef]
13. Polizzotto, C. A gradient elasticity theory for second-grade materials and higher order inertia. *Int. J. Solids Struct.* **2012**, *49*, 2121–2137. [CrossRef]
14. Dontsov, E.V.; Tokmashev, R.D.; Guzina, B.B. A physical perspective of the length scales in gradient elasticity through the prism of wave dispersion. *Int. J. Solids Struct.* **2013**, *50*, 3674–3684. [CrossRef]
15. Koiter, W. Couple stresses in the theory of elasticity, I and II. *Roy. Neth. Acad. Sci. B* **1964**, *67*, 0964.
16. Mindlin, R.; Tiersten, H. Effects of couple-stresses in linear elasticity. *Arch. Ration. Mech. Anal.* **1962**, *11*, 415–448. [CrossRef]
17. Mindlin, R.; Eshel, N. On first strain-gradient theories in linear elasticity. *Int. J. Solids Struct.* **1968**, *4*, 109–124. [CrossRef]
18. Mindlin, R.D. Second gradient of strain and surface-tension in linear elasticity. *Int. J. Solids Struct.* **1965**, *1*, 417–438. [CrossRef]
19. Toupin, R.A. Theories of elasticity with couple-stress. *Arch. Ration. Mech. Anal.* **1964**, *17*, 85–112. [CrossRef]
20. Aifantis, E.C. On the role of gradients in the localization of deformation and fracture. *Int. J. Eng. Sci.* **1992**, *30*, 1279–1299. [CrossRef]
21. Ru, C.Q.; Aifantis, E.C. A simple approach to solve boundary-value problems in gradient elasticity. *Acta Mech.* **1993**, *101*, 59–68. [CrossRef]
22. Askes, H.; Aifantis, E.C. Gradient elasticity in statics and dynamics: An overview of formulations, length scale identification procedures, finite element implementations and new results. *Int. J. Solids Struct.* **2011**, *48*, 1962–1990. [CrossRef]
23. Cordero, N.M.; Forest, S.; Busso, E.P. Second strain gradient elasticity of nano-objects. *J. Mech. Phys. Solids* **2016**, *97*, 92–124. [CrossRef]
24. Kong, S.; Zhou, S.; Nie, Z.; Wang, K. Static and dynamic analysis of micro beams based on strain gradient elasticity theory. *Int. J. Eng. Sci.* **2009**, *47*, 487–498. [CrossRef]
25. Malikan, M.; Eremeyev, V.A. On the Dynamics of a Visco–Piezo–Flexoelectric Nanobeam. *Symmetry* **2020**, *12*, 643. [CrossRef]
26. Wang, B.; Zhao, J.; Zhou, S. A micro scale Timoshenko beam model based on strain gradient elasticity theory. *Eur. J. Mech. A/Solids* **2010**, *29*, 591–599. [CrossRef]
27. Zhang, B.; He, Y.; Liu, D.; Gan, Z.; Shen, L. Size-dependent functionally graded beam model based on an improved third-order shear deformation theory. *Eur. J. Mech. A/Solids* **2014**, *47*, 211–230. [CrossRef]
28. Papargyri-Beskou, S.; Giannakopoulos, A.; Beskos, D. Variational analysis of gradient elastic flexural plates under static loading. *Int. J. Solids Struct.* **2010**, *47*, 2755–2766. [CrossRef]
29. Wang, B.; Zhou, S.; Zhao, J.; Chen, X. A size-dependent Kirchhoff micro-plate model based on strain gradient elasticity theory. *Eur. J. Mech. A/Solids* **2011**, *30*, 517–524. [CrossRef]
30. Ma, H.; Gao, X.-L.; Reddy, J. A non-classical Mindlin plate model based on a modified couple stress theory. *Acta Mech.* **2011**, *220*, 217–235. [CrossRef]
31. Ke, L.-L.; Wang, Y.-S.; Yang, J.; Kitipornchai, S. Free vibration of size-dependent Mindlin microplates based on the modified couple stress theory. *J. Sound Vib.* **2012**, *331*, 94–106. [CrossRef]
32. Zhang, B.; He, Y.; Liu, D.; Shen, L.; Lei, J. An efficient size-dependent plate theory for bending, buckling and free vibration analyses of functionally graded microplates resting on elastic foundation. *Appl. Math. Model.* **2015**, *39*, 3814–3845. [CrossRef]

33. Zhang, B.; He, Y.; Liu, D.; Shen, L.; Lei, J. Free vibration analysis of four-unknown shear deformable functionally graded cylindrical microshells based on the strain gradient elasticity theory. *Compos. Struct.* **2015**, *119*, 578–597. [CrossRef]
34. Papargyri-Beskou, S.; Beskos, D. Stability analysis of gradient elastic circular cylindrical thin shells. *Int. J. Eng. Sci.* **2009**, *47*, 1379–1385. [CrossRef]
35. Roudbari, M.A.; Jorshari, T.D.; Lü, C.; Ansari, R.; Kouzani, A.Z.; Amabili, M. A review of size-dependent continuum mechanics models for micro-and nano-structures. *Thin-Walled Struct.* **2022**, *170*, 108562. [CrossRef]
36. Kong, S. A Review on the Size-Dependent Models of Micro-beam and Micro-plate Based on the Modified Couple Stress Theory. *Arch. Comput. Methods Eng.* **2021**, *29*, 1–31. [CrossRef]
37. Lim, C.; Zhang, G.; Reddy, J. A higher-order nonlocal elasticity and strain gradient theory and its applications in wave propagation. *J. Mech. Phys. Solids* **2015**, *78*, 298–313. [CrossRef]
38. Eringen, A.C. Nonlocal polar elastic continua. *Int. J. Eng. Sci.* **1972**, *10*, 1–16. [CrossRef]
39. Lu, L.; Guo, X.; Zhao, J. A unified nonlocal strain gradient model for nanobeams and the importance of higher order terms. *Int. J. Eng. Sci.* **2017**, *119*, 265–277. [CrossRef]
40. Lu, L.; Guo, X.; Zhao, J. Size-dependent vibration analysis of nanobeams based on the nonlocal strain gradient theory. *Int. J. Eng. Sci.* **2017**, *116*, 12–24. [CrossRef]
41. Lu, L.; Guo, X.; Zhao, J. On the mechanics of Kirchhoff and Mindlin plates incorporating surface energy. *Int. J. Eng. Sci.* **2018**, *124*, 24–40. [CrossRef]
42. Atashafrooz, M.; Bahaadini, R.; Sheibani, H.R. Nonlocal, strain gradient and surface effects on vibration and instability of nanotubes conveying nanoflow. *Mech. Adv. Mater. Struct.* **2018**, *27*, 586–598. [CrossRef]
43. Sahmani, S.; Aghdam, M.M. Nonlocal strain gradient shell model for axial buckling and postbuckling analysis of magneto-electro-elastic composite nanoshells. *Compos. Part B Eng.* **2018**, *132*, 258–274. [CrossRef]
44. Ma, L.H.; Ke, L.L.; Reddy, J.N.; Yang, J.; Kitipornchai, S.; Wang, Y.S. Wave propagation characteristics in magneto-electro-elastic nanoshells using nonlocal strain gradient theory. *Compos. Struct.* **2018**, *199*, 10–23. [CrossRef]
45. Lu, L.; Guo, X.; Zhao, J. A unified size-dependent plate model based on nonlocal strain gradient theory including surface effects. *Appl. Math. Model.* **2019**, *68*, 583–602. [CrossRef]
46. Chen, W.; Wang, L.; Dai, H. Stability and Nonlinear Vibration Analysis of an Axially Loaded Nanobeam Based on Nonlocal Strain Gradient Theory. *Int. J. Appl. Mech.* **2019**, *11*, 1950069. [CrossRef]
47. Zhang, B.; Shen, H.; Liu, J.; Wang, Y.; Zhang, Y. Deep postbuckling and nonlinear bending behaviors of nanobeams with nonlocal and strain gradient effects. *Appl. Math. Mech.* **2019**, *40*, 515–548. [CrossRef]
48. Lu, L.; Zhu, L.; Guo, X.; Zhao, J.; Liu, G. A nonlocal strain gradient shell model incorporating surface effects for vibration analysis of functionally graded cylindrical nanoshells. *Appl. Math. Mech.* **2019**, *40*, 1695–1722. [CrossRef]
49. Xu, X.-J.; Deng, Z.-C.; Meng, J.-M.; Zhang, K. Bending and vibration analysis of generalized gradient elastic plates. *Acta Mech.* **2014**, *225*, 3463–3482. [CrossRef]
50. Qi, L.; Zhou, S. A size-dependent spherical microshell model based on strain gradient elasticity theory. *Eur. J. Mech. A/Solids* **2020**, *84*, 104087. [CrossRef]
51. Movassagh, A.A.; Mahmoodi, M.J. A micro-scale modeling of Kirchhoff plate based on modified strain-gradient elasticity theory. *Eur. J. Mech. A/Solids* **2013**, *40*, 50–59. [CrossRef]
52. Wang, B.; Huang, S.; Zhao, J.; Zhou, S. Reconsiderations on boundary conditions of Kirchhoff micro-plate model based on a strain gradient elasticity theory. *Appl. Math. Model.* **2016**, *40*, 7303–7317. [CrossRef]
53. Thai, S.; Thai, H.T.; Vo, T.P.; Patel, V.I. Size-dependant behaviour of functionally graded microplates based on the modified strain gradient elasticity theory and isogeometric analysis. *Comput. Struct.* **2017**, *190*, 219–241. [CrossRef]
54. Nguyen, H.X.; Atroshchenko, E.; Ngo, T.; Nguyen-Xuan, H.; Vo, T.P.J.E.S. Vibration of cracked functionally graded microplates by the strain gradient theory and extended isogeometric analysis. *Eng. Struct.* **2019**, *187*, 251–266. [CrossRef]
55. Nguyen, H.X.; Atroshchenko, E.; Nguyen-Xuan, H.; Vo, T.P. Geometrically nonlinear isogeometric analysis of functionally graded microplates with the modified couple stress theory. *Comput. Struct.* **2017**, *193*, 110–127. [CrossRef]
56. Nguyen, H.X.; Nguyen, T.N.; Abdel-Wahab, M.; Bordas, S.; Nguyen-Xuan, H.; Vo, T.P. A refined quasi-3D isogeometric analysis for functionally graded microplates based on the modified couple stress theory. *Comput. Methods Appl. Mech. Eng.* **2017**, *313*, 904–940. [CrossRef]
57. Niiranen, J.; Kiendl, J.; Niemi, A.H.; Reali, A. Isogeometric analysis for sixth-order boundary value problems of gradient-elastic Kirchhoff plates. *Comput. Methods Appl. Mech. Eng.* **2017**, *316*, 328–348. [CrossRef]
58. Balobanov, V.; Kiendl, J.; Khakalo, S.; Niiranen, J. Kirchhoff–Love shells within strain gradient elasticity: Weak and strong formulations and an H3-conforming isogeometric implementation. *Comput. Methods Appl. Mech. Eng.* **2019**, *344*, 837–857. [CrossRef]
59. Babu, B.; Patel, B. A new computationally efficient finite element formulation for nanoplates using second-order strain gradient Kirchhoff's plate theory. *Compos. Part B Eng.* **2019**, *168*, 302–311. [CrossRef]
60. Wang, X. Novel differential quadrature element method for vibration analysis of hybrid nonlocal Euler–Bernoulli beams. *Appl. Math. Lett.* **2018**, *77*, 94–100. [CrossRef]
61. Ishaquddin, M.; Gopalakrishnan, S. A novel weak form quadrature element for gradient elastic beam theories. *Appl. Math. Model.* **2020**, *77*, 1–16. [CrossRef]

62. Zhang, B.; Li, H.; Kong, L.; Wang, J.; Shen, H. Strain gradient differential quadrature beam finite elements. *Comput. Struct.* **2019**, *218*, 170–189. [CrossRef]
63. Zhang, B.; Li, H.; Kong, L.; Zhang, X.; Feng, Z. Weak-form differential quadrature finite elements for functionally graded micro-beams with strain gradient effects. *Acta Mech.* **2021**, *232*, 4009–4036. [CrossRef]
64. Zhang, B.; Li, H.; Kong, L.; Shen, H.; Zhang, X. Size-dependent static and dynamic analysis of Reddy-type micro-beams by strain gradient differential quadrature finite element method. *Thin-Walled Struct.* **2020**, *148*, 106496. [CrossRef]
65. Zhang, B.; Li, H.; Kong, L.; Shen, H.; Zhang, X. Size-dependent vibration and stability of moderately thick functionally graded micro-plates using a differential quadrature-based geometric mapping scheme. *Eng. Anal. Bound. Elem.* **2019**, *108*, 339–365. [CrossRef]
66. Zhang, B.; Li, H.; Kong, L.; Zhang, X.; Feng, Z. Strain gradient differential quadrature finite element for moderately thick micro-plates. *Int. J. Numer. Methods Eng.* **2020**, *121*, 5600–5646. [CrossRef]
67. Bo, Z.; Li, H.; Kong, L.; Zhang, X.; Shen, H. Strain gradient differential quadrature Kirchhoff plate finite element with the C2 partial compatibility. *Eur. J. Mech. A/Solids* **2020**, *80*, 103879.
68. Zhang, B.; Li, H.; Liu, J.; Shen, H.; Zhang, X. Surface energy-enriched gradient elastic Kirchhoff plate model and a novel weak-form solution scheme. *Eur. J. Mech. A/Solids* **2021**, *85*, 104118. [CrossRef]
69. Zhang, B.; Li, H.; Kong, L.; Zhang, X.; Feng, Z. Variational formulation and differential quadrature finite element for freely vibrating strain gradient Kirchhoff plates. *ZAMM-J. Appl. Math. Mech.* **2021**, *101*, e202000046. [CrossRef]
70. Duan, Y.; Zhang, B.; Li, X.; Zhang, X.; Shen, H. Size-Dependent Elastic Buckling of Two-Variable Refined Microplates Embedded in Elastic Medium. *Int. J. Appl. Mech.* **2022**, *14*, 2250039. [CrossRef]
71. Liew, K.-M.; Xiang, Y.; Kitipornchai, S.; Wang, C. *Vibration of Mindlin Plates: Programming the p-Version Ritz Method*; Elsevier: Oxford, UK, 1998.